Chemical Science

ROYAL SOCIETY OF CHEMISTRY

PERSPECTIVE

View Article Online
View Journal | View Issue

Cite this: *Chem. Sci.*, 2025, **16**, 14424

All publication charges for this article have been paid for by the Royal Society of Chemistry

Received 30th April 2025
Accepted 18th July 2025

DOI: 10.1039/d5sc03154k

rsc.li/chemical-science

Polythiophenes as electron donors in organic solar cells

Xiyue Yuan,[a] Jianglong Li,[a] Wanting Deng,[a] Xia Zhou[b] and Chunhui Duan *[a]

Recent advancements in organic solar cells (OSCs) highlight the critical need for low-cost, readily available polymer donors to facilitate the commercialization of OSCs. Among the various photovoltaic materials, polythiophene (PT) and its derivatives have emerged as the most promising candidates for commercial applications, primarily due to their affordability and ease of scalable synthesis. Over the past few years, the combination of PTs with nonfullerene acceptors (NFAs) has led to significant improvements in photovoltaic efficiency. This paper provides a comprehensive overview of design strategies for polythiophene electron donors utilized in NFA-based OSCs, focusing on the modulation of energy levels and aggregation properties. It also evaluates recent progress in optimizing film morphology in PT:NFA blends, emphasizing key factors such as donor–acceptor miscibility, solution-state aggregation control, and film-formation kinetics. Additionally, the paper explores the applications of PTs in all-polymer OSCs and large-area OSCs and the stability of PT-based OSCs. Finally, the paper addresses scientific challenges associated with PT-based OSCs, aiming to provide guidance and stimulate new ideas for further research.

1. Introduction

Organic solar cells (OSCs) exhibit significant economic potential owing to their unique features, including flexibility, lightweight, and compatibility with large-scale fabrication *via* solution processing.[1–5] Recent advancements in novel nonfullerene acceptors (NFAs) have driven remarkable progress in power conversion efficiencies (PCEs),[6–10] now exceeding 20%,[11–13] approaching the threshold for practical commercialization. However, despite these improvements in device efficiency, cost remains a key barrier to widespread OSC commercialization.[14–16] Most high-efficiency polymer donors, such as PM6 (ref. 17) and D18 (ref. 18) (Fig. 1a), are predominantly utilized donor–acceptor (D–A) alternating conjugated polymers.[19–21] These materials often incorporate expensive functional groups and fused heterocyclic compounds, leading to complex synthesis and purification processes,[22–24] which

[a]*Institute of Polymer Optoelectronic Materials and Devices, Guangdong Basic Research Center of Excellence for Energy & Information Polymer Materials, State Key Laboratory of Luminescent Materials and Devices, South China University of Technology, China. E-mail: duanchunhui@scut.edu.cn*

[b]*School of New Energy, Ningbo University of Technology, China*

Xiyue Yuan

Xiyue Yuan is currently a postdoctoral researcher in the group of Prof. Chunhui Duan at the South China University of Technology. She received her PhD degree from the South China University of Technology under the supervision of Prof. Chunhui Duan in 2023. Her major is the synthesis of conjugated polymers and applications in organic solar cells.

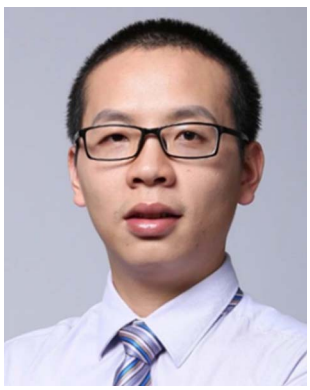

Chunhui Duan

Chunhui Duan received his bachelor's degree from the Dalian University of Technology in 2008 and PhD degree from the South China University of Technology in 2013. After a postdoc training at the Eindhoven University of Technology, he joined the South China University of Technology as a full professor in 2017. His research interests focus on organic semiconductors and their application in solar cells and photodetectors.

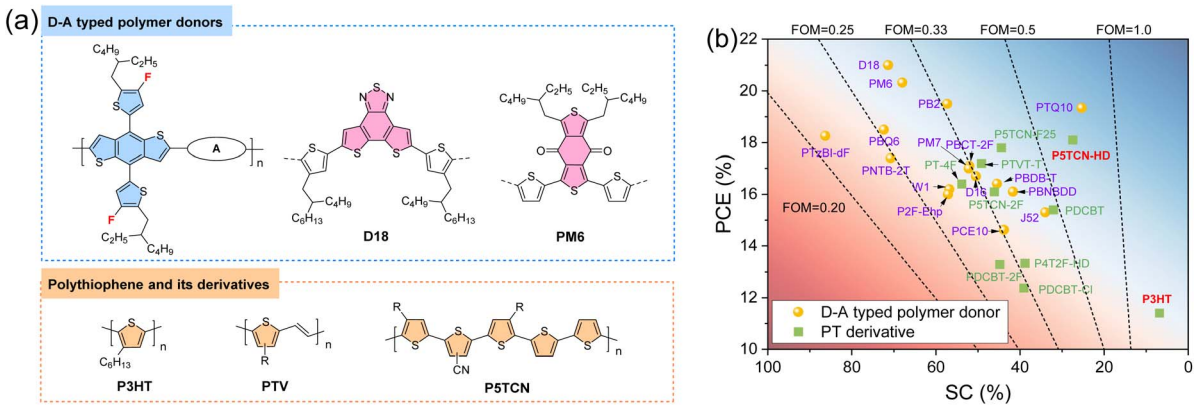

Fig. 1 (a) Chemical structures of D18 and PM6 and the backbones of polythiophene (PT) and its derivatives. (b) Summary of the power conversion efficiencies (PCEs) and synthetic complexity (SC) of D–A typed polymer donors and polythiophene derivatives. The SC of polymer donors is assessed through five parameters: (1) the number of synthetic steps (NSS), (2) the reciprocal yields (RY) of the monomers, (3) the number of unit operations (NUO) required for the isolation/purification of the monomers, (4) the number of column chromatographic (NCC) purifications required by the monomers, and (5) the number of hazardous chemicals (NHC) used for their preparation, and it can be calculated according to the protocol established by Po *et al.*[14] From SC and PCE, a figure of merit (FOM = PCE/SC) can be calculated which best represents the cost-efficiency balance of a given donor material.

severely limit the large-scale industrial manufacturing of OSCs.[25–27]

Polythiophenes (PTs), characterized by their fully thiophene-based backbone connected by single or double bonds, or heteroatom-substituted polythiophene analogs, have long been recognized as cost-effective and industrially scalable materials for OSCs.[27–29] These polymers have served as benchmark electron donors in OSC research, owing to their exceptional crystallinity, high hole mobility, and synthetic accessibility (Fig. 1b).[30] However, the prominence of PTs has been challenged by the emergence of fused-ring copolymer donors, largely due to the lagged device performance caused by their high-lying energy levels[31,32] and uncontrollable aggregation behaviors.[33,34] In recent years, PT-based donors have regained research attention in OSCs, motivated by the growing commercialization demands for cost-effective materials. Concurrent advancements in molecular design and device engineering have facilitated precise modulation of the energy levels and aggregation behaviors of these low-cost polymers, achieving PCEs exceeding 18%, which demonstrates the potential to perform comparably to their structurally complex counterparts.[35,36] To fully realize the potential of PT:NFA systems, it is essential to establish a comprehensive understanding of the blends from the perspectives of molecular design and device optimization.

This paper provides a comprehensive summary of recent advancements in PT-based OSCs. We first discuss the new synthetic methods and molecular design strategies that enable precise control of energy levels and aggregation behaviors of PTs. Subsequently, we analyze critical advances in morphology optimization and device engineering for PT:NFA blends, focusing on three key aspects: (1) donor–acceptor miscibility, (2) aggregation regulation in the solution-state, and (3) film formation kinetics. Finally, we explore the application of PTs in all-polymer and large-area OSCs, along with the device stability for PT-based OSCs. By elucidating fundamental design principles in molecular design and morphology control, this paper aims to promote the development of commercially viable and environmentally friendly OSC technologies.

2. Molecular engineering of polythiophenes

2.1 New synthetic methods of polythiophenes

Poly(3-hexylthiophene) (P3HT), the most widely used polythiophene, can be synthesized in kilogram quantities even within the confines of a research laboratory. It is typically produced by the traditional Grignard metathesis (GRIM) method, which utilizes a nickel catalyst through Kumada catalyst-transfer polycondensation (KCTP) (Fig. 2a).[37,38] In contrast to step-growth polycondensation methods, such as Suzuki or Stille coupling, KCTP proceeds *via* a chain-growth mechanism,[39] enabling precise control of molecular weights, defined end-group functionality, and outstanding synthetic reproducibility. Nevertheless, this methodology requires organometallic reagents, which will introduce additional synthetic steps and generate stoichiometric byproducts, thereby conflicting with the principles of green chemistry.

In 2020, Rangel *et al.* reported a series of regioregular P3HTs (RR-P3HTs) by optimizing an eco-friendly direct arylation polymerization (DArP) method. The highest PCEs of 3.6% and 3.4% were achieved with P3HTs of the highest RR (94 and 93%), corresponding to the lowest number-average molecular weight (M_n) of 5.1 and 4.9 kg mol^{-1}.[40] In 2021, Liu *et al.* synthesized five batches of P3HT *via* DArP (Fig. 2a), with M_n values ranging from 6.0 to 35.9 kg mol^{-1}. The DArP process utilized 2-bromo-3-hexylthiophene as the monomer, with the Herrmann catalyst as the palladium source, Cs_2CO_3 as the base and tetrahydrofuran (THF) as the solvent. Due to the optimal π–π crystalline ordering and favorable morphological characteristics, the P3HT

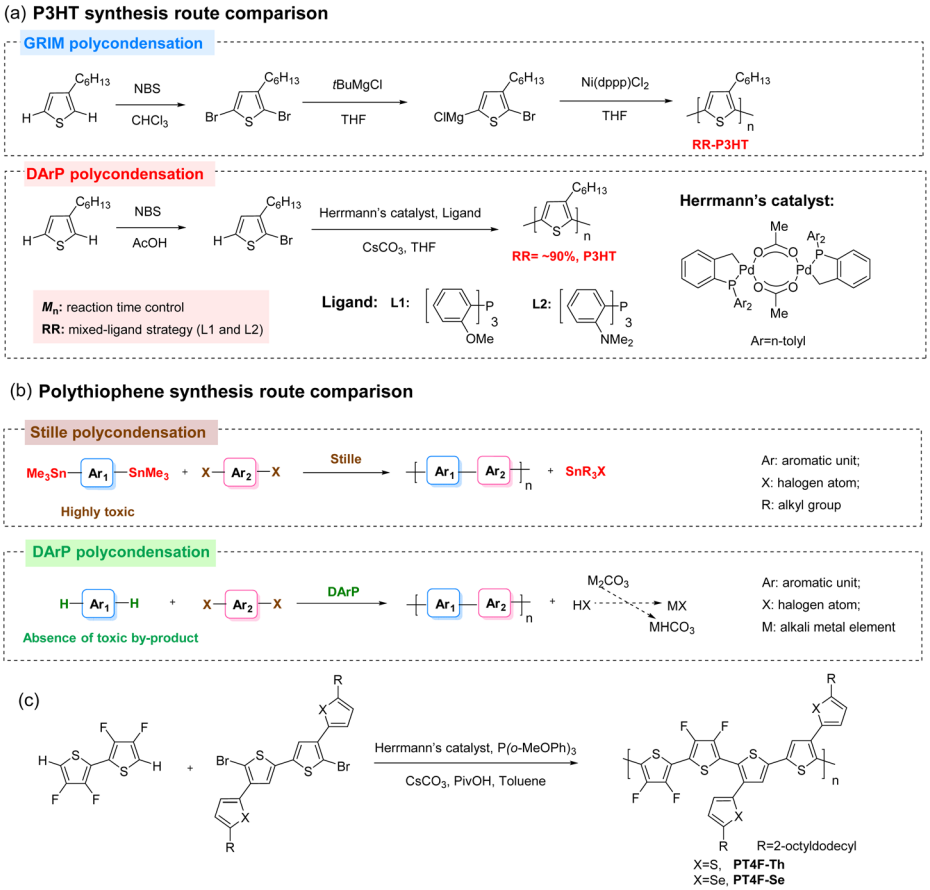

Fig. 2 (a) Comparison of the synthetic routes to P3HT *via* Grignard metathesis (GRIM)[37] and direct arylation polycondensation (DArP).[41] (b) Comparison of the synthetic routes to polythiophene *via* Stille polycondensation and DArP. Notably, the protons generated during the C–H activation process are neutralized by the carbonate base additive, resulting in the formation of non-toxic salt compounds.[46] (c) The synthesis of PT4F-Th and PT4F-Se *via* the DArP method.[46]

based on the medium M_n batch (17.2 kg mol^{-1}) achieved a champion PCE of 9.6%, which was the highest value reported for P3HT-based OSCs at that time.[41]

In 2022, Liu *et al.* employed the DArP protocol to synthesize a wide range of poly(3-alkylthiophenes) with varied side-chain lengths (from butyl to octyl) and revealed its impact on molecular packing and charge transport behaviors. The odd-even effect was clearly observed in poly(3-alkylthiophene):ZY-4Cl blend films, where poly(3-alkylthiophene) with odd-numbered chains showed stronger π–π stacking due to enhanced van der Waals interactions. The solar cell based on poly(3-pentylthiophene) (P3PT) achieved a higher PCE of 9.79% and a fill factor (FF) of 70.8%.[42]

Despite progress in DArP-synthesized P3HT, the regioregularity (RR) of the optimized batches remains limited to 90%, which is still significantly below the typical RR values required for high-performance OSCs.[43,44] In 2022, Liu *et al.* reported a simple mixed-ligand strategy to precisely modulate the RR of P3HT (Fig. 2a). Density functional theory (DFT) calculations revealed that the ligand tris(2-methoxyphenyl)phosphine (L2) could suppress the formation of head-to-head (H–H) and tail-to-tail (T–T) linkages, thereby enhancing the RR of P3HT. By tuning the molar ratio of ligands 2,2′,2″-phosphinidynetris[*N*,*N*-dimethylbenzenamine] (L1) and L2, four batches of P3HT with controlled RR (90–98%) were obtained. The OSC based on P3HT with a RR of 95% achieved a record PCE of 10.82%, which was the highest value for P3HT-based OSCs at that time.[45]

Compared to P3HT, polythiophene derivatives have emerged as more appealing donor materials in OSCs due to their complementary light absorption, matched energy levels and appropriate miscibility with prevailing NFAs. However, the top-performance P3HT derivatives were typically synthesized *via* Stille polycondensation, which suffers from significant toxicity and poor atom economy (Fig. 2b).[47] In contrast, DArP presents an attractive alternative by enabling C–H/C–X coupling without organostannane monomers.[48,49] However, the PCEs of DArP-derived donor polymers are significantly lower than those of their Stille-synthesized counterparts.[50] This is due to the stringent criteria for monomer selection imposed by DArP,[51] as only monomers with highly reactive and selective C–H bonds can be readily converted into defect-free conjugated polymers. Directly applying this method to the synthesis of reported donor materials may result in structural defects, thereby compromising their performance.

To address this issue, Menda *et al.* in 2020 developed a series of ester-functionalized polythiophenes (P3OETs) *via* the palladium-catalyzed DArP method, with M_n ranging from 9.0 to 27.0 kg mol^{-1}. Their work demonstrated a systematic decrease in ionization potentials and optical bandgaps as the head-to-tail (HT) ratios increased, which is attributed to enhanced backbone coplanarity and π-electron delocalization.[52] In 2024, Zhang *et al.* selected a highly reactive monomer 3,3′,4,4′-tetrafluoro-2,2′-bithiophene (4FBT) to develop a new DArP-derived polythiophene donor (PT4F-Th). The tetrafluoro and thiophene-based conjugated side chains in PT4F-Th ensured both high device performance and excellent feasibility for DArP-synthesis. Combined with the delicate control of film morphology, PT4F-Th achieved a PCE of 16.4% in OSCs with BTP-eC9, which is comparable to that of the top-performing polythiophenes prepared *via* Stille polycondensation.[46]

2.2 Design of polythiophenes

Derived from the strong electron-rich characteristics of the thiophene ring, PTs usually present relatively high-lying highest occupied molecular orbital (HOMO) energy levels. Given that open-circuit voltage (V_{oc}) of OSCs is directly related to the energy offset between the lowest unoccupied molecular orbital (LUMO) energy level of the acceptor and the HOMO energy level of the donor, the high-lying HOMO energy level of PTs will cause the difficulty in obtaining high V_{oc}, thereby constraining PCEs for PT-based OSCs. Additionally, PT-based OSCs usually suffered from unfavorable active layer morphology due to the undesirable aggregation behaviors of PTs, thus limiting the short-circuit current density (J_{sc}) and FF. Attaching electron-withdrawing groups onto the thiophene unit is a common approach to construct PTs with downshifted energy levels and enhanced interchain π–π interactions.

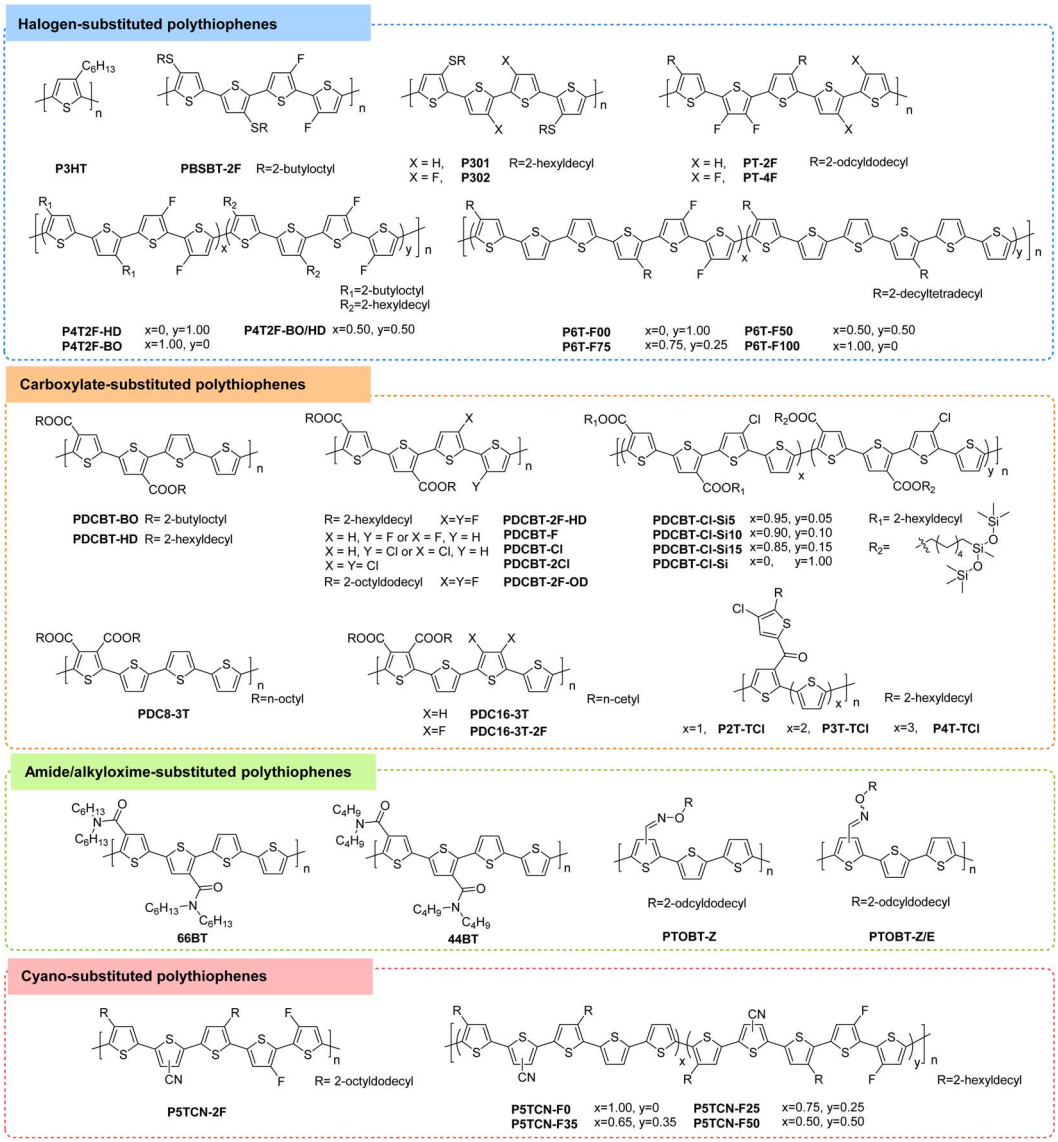

Fig. 3 The chemical structures of polythiophenes.

2.2.1 Halogen-substituted polythiophenes. Halogen substitution is a common strategy to lower the HOMO energy levels of PTs (Fig. 3). In 2019, our group introduced fluorine atoms into a polythiophene backbone and developed three novel polythiophenes (P4T2F-HD, P4T2F-HD/BO, and P4T2F-BO). These polythiophenes exhibited down-shifted HOMO energy levels (~−5.30 eV), excellent coplanarity and optimal solution aggregation characteristics.[53] When combined with non-fullerene acceptor O-IDTBR, the OSC based on P4T2F-HD achieved a maximum PCE of 7.0% (Table 1). When Y6-BO (Fig. 4) was employed as an acceptor, P4T2F-HD further yielded a new record PCE of 13.65%.[54] Following this work, our group further systematically investigated the effect of fluorination degrees (P6T-F00, P6T-F50, P6T-F75, and P6T-F100) on device performance of OSCs.[55] Increasing the fluorination degree within the PT backbone improved the polymer crystallinity, absorption coefficients, and relative dielectric constants. When blended with acceptor EH-IDTBR, the PCE increased from 4.3% for P6T-F00 to 7.3% for P6T-F100. To finely tune the energy levels of PT, Xu *et al.* incorporated alkylthio and fluorine groups into the polythiophene backbone and reported a new PT, PBSBT-2F. The OSC based on PBSBT-2F:ITIC achieved a PCE of 6.7% with a V_{oc} of 0.75 V.[56] In 2021, Yuan *et al.* reported a new fluorinated polythiophene P302. In comparison to its non-fluorinated counterpart P301, fluorination in P302 can not only downshift the energy levels, but also improve the phase separation of the active layers, which further contributed to the enhanced PCE (9.65% *versus* 2.33%) in the resulting OSC.[57] In 2022, Jeong *et al.* developed two fluorinated polythiophene donors, PT-2F and PT-4F, with two or four fluorine atoms in their repeating units.[58] The deeper-lying HOMO energy level and enhanced crystallinity of PT-4F contributed to higher V_{oc} (0.83

Table 1 Energy levels and photovoltaic parameters of polythiophenes

Polymer	HOMO/LUMO (eV)	Acceptor	V_{oc} (V)	J_{sc} (mA cm^{-2})	FF	PCE (%)	Ref.
P4T2F-BO	−5.30/−3.40	O-IDTBR	1.06	9.9	60	6.3	53
P4T2F-BO/HD	−5.31/−3.40	O-IDTBR	1.02	10.7	60	6.5	53
P4T2F-HD	−5.35/−3.43	O-IDTBR	1.04	10.0	67	7.0	53
		Y6-BO	0.72	24.39	75.30	13.65	54
P6T-F00	−5.28/−3.28	EH-IDTBR	1.07	7.0	57	4.3	55
P6T-F50	−5.27/−3.30	EH-IDTBR	1.00	8.5	63	5.3	55
P6T-F75	−5.26/−3.30	EH-IDTBR	0.98	11.0	64	6.9	55
P6T-F100	−5.25/−3.33	EH-IDTBR	0.99	11.2	66	7.3	55
PBSBT-2F	−5.06/−2.79	ITIC	0.75	13.5	66.6	6.7	56
P301	−5.02/−3.18	Y5	0.72	9.67	33	2.33	57
P302	−5.12/−3.29	Y5	0.84	20.24	57	9.65	57
PT-2F	−5.48/−3.45	BTP-eC9	0.77	23.97	65	12.0	58
PT-4F	−5.58/−3.52	BTP-eC9	0.83	24.69	76	15.6	58
		BTP-eC9:L8-BO	0.84	25.27	77	16.4	58
PDCBT-BO	−5.31/−3.00	ITIC	0.94	16.50	65.67	10.16	59
PDCBT-2F-HD	−5.59/−3.69	IT-M	1.13	10.43	55.7	6.6	60
PDCBT-2F-OD	−5.60/−3.67	IT-4F	0.92	17.8	69	11.6	32
PDC8-3T	−5.32/−3.38	ITIC-4F	0.76	3.32	27.3	0.69	61
PDC16-3T	−5.36/−3.42	ITIC-4F	0.82	5.58	39.1	1.79	61
PDC16-3T-2F	−5.38/−3.48	ITIC-4F	0.85	14.60	58.4	7.21	61
PDCBT-HD	−5.20/−2.90	ITIC-Th1	0.89	16.60	55.2	8.14	62
PDCBT-F	−5.32/−2.98	ITIC-Th1	0.93	17.52	66.2	10.85	62
PDCBT-2F	−5.40/−3.03	ITIC-Th1	0.98	15.32	56.5	8.48	62
PDCBT-Cl	−5.34/−3.01	ITIC-Th1	0.94	18.50	71.2	12.38	62
PDCBT-2Cl	−5.44/−3.00	ITIC-Th1	0.99	13.54	51.8	6.94	62
PDCBT-Cl-Si5	−5.34/−3.01	ITIC-Th1	0.93	19.27	71.7	12.85	63
PDCBT-Cl-Si10	−5.34/−3.01	ITIC-Th1	0.92	18.55	71.4	12.19	63
PDCBT-Cl-Si15	−5.34/−3.01	ITIC-Th1	0.91	17.45	66.0	10.48	63
PDCBT-Cl-Si	−5.34/−3.01	ITIC-Th1	0.89	10.19	45.3	4.11	63
P2T-TCl	−5.37/−3.49	Y6-BO	0.86	13.33	45.8	5.25	64
P3T-TCl	−5.17/−3.34	Y6-BO	0.78	15.62	46.1	5.62	64
P4T-TCl	−5.10/−3.29	Y6-BO	0.73	19.61	63.9	9.15	64
44BT	−5.30/−3.22	ITIC-4F	0.81	3.5	30	0.85	75
PTOBT-*Z*	−5.43/−3.49	ITIC	0.82	19.86	55	9.04	66
PTOBT-*Z*/*E*	−5.44/−3.51	ITIC	0.83	16.56	50	6.86	66
P5TCN-2F	−5.54/−3.65	Y6	0.85	25.07	75.0	16.1	71
P5TCN-F0	−5.41/−3.52	Y6	0.81	20.83	68.8	11.5	35
(P5TCN-HD)		eC9-2Cl	0.87	25.23	77.93	17.10	72
		eC9-2Cl:L8-BO-F	0.87	26.18	79.17	18.12	72
P5TCN-F25	−5.44/−3.56	Y6	0.79	27.13	77.1	16.6	35
		Y6:$PC_{71}BM$	0.80	27.55	77.7	17.2	35
P5TCN-F35	−5.48/−3.60	Y6	0.80	26.87	75.0	16.1	35
P5TCN-F50	−5.50/−3.63	Y6	0.82	24.78	72.0	14.6	35

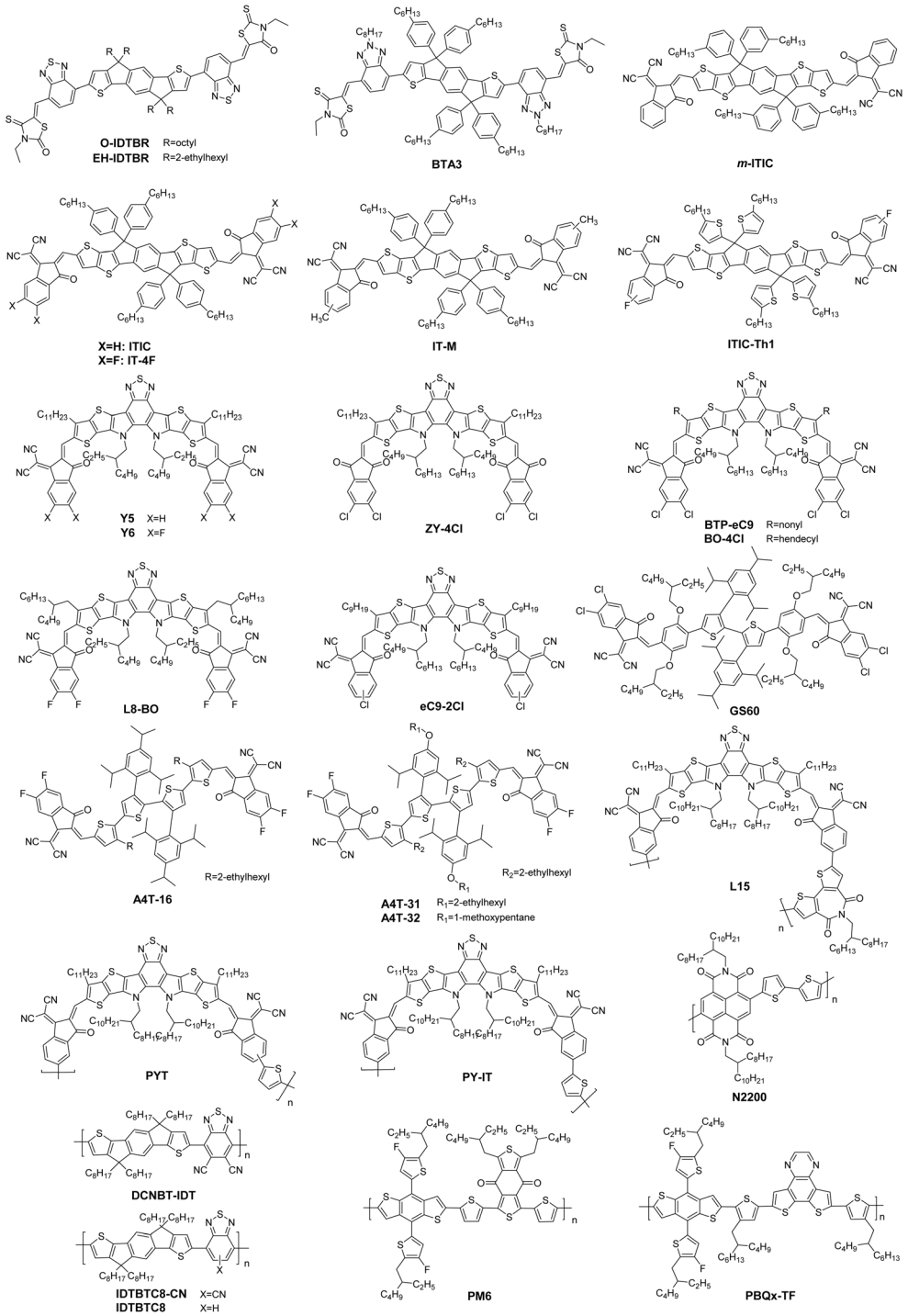

Fig. 4 The chemical structures of the nonfullerene acceptors and fused-ring polymer donors involved in this paper.

V) and FF (76%), which resulted in a PCE of 15.6% in PT-4F:BTP-eC9-based OSCs. When L8-BO with a shallow-lying LUMO energy level was employed as the third component, a higher PCE of 16.4% was achieved for ternary OSCs.

2.2.2 Carboxylate-substituted polythiophenes. Introducing electron-withdrawing carboxylate groups is another effective strategy to improve the photovoltaic performance of PTs. In 2014, Zhang *et al.* developed a carboxylate-functionalized PT derivative, PDCBT.[31] The carboxylate substituents pushed the HOMO energy level down by ≈0.30 eV with respect to P3HT. When [6,6]-phenyl-C71-butyric acid methyl ester ($PC_{71}BM$) was employed as an acceptor, the PDCBT-based OSC achieved an excellent PCE of 7.65%.[31] With ITIC as an acceptor, the OSC based on PDCBT further yielded a higher PCE of 10.16% with a high V_{oc} of 0.94 V.[59] Subsequently, in pursuit of OSCs with higher V_{oc}, a new fluorinated PBDCT derivative (named PDCBT-

2F) with a lower HOMO energy level of −5.6 eV was synthesized by the same group.[60] The OSC based on PBDCT-2F:IT-M exhibited a PCE of 6.6% with a high V_{oc} of 1.13 V and low energy loss (E_{loss}) of 0.46 eV. When blended with IT-4F, which shows broader absorption than IT-M, the PCE of PDCBT-2F-based OSC was further improved to 11.6%.[32] Recently, Su *et al.* reported a series of PTs (PDC8-3T, PDC16-3T, and PDC16-3T-2F) featuring two ester side chains in the PT backbone. The incorporation of the thiophene π-spacer reduced the steric hindrance, while elongated alkyl side chains improved solubility and processability. With ITIC-4F as an acceptor, the OSC based on PDC16-3T-2F yielded the highest PCE of 7.21%.[61]

Considering that chlorinated polymers can be synthesized more readily than their fluorinated counterparts, in 2019, Wang *et al.* explored this approach in PTs by developing two new chlorinated PTs (PDCBT-Cl and PDCBT-2Cl).[62] Owing to the proper phase-separated morphology with favorable molecular packing, the OSC based on PDCBT-Cl achieved a PCE of 12.38%, which was the highest reported value for PTs at that time. To finely optimize the miscibility of PT:NFA blend systems, Wang *et al.* further reported a series of ester-substituted PTs (PDCBT-Cl-Six) by incorporating varying amounts (5–15%) of siloxane side chains. This systematic variation allowed for the fine-tuning of compatibility and phase separation morphology within PT:NFA blend systems. Notably, the device based on PDCBT-Cl-Si5 achieved the highest PCE of 12.85%.[63] In 2025, Cao *et al.* attached an electron-deficient chloro-substituted thenoyl side chain to the PT backbone and reported three PTs (P2T-TCl, P3T-TCl and P4T-TCl) with deep HOMO energy levels down to ∼−5.37 eV. As the number of thiophenes in each repeat unit increased, more ordered molecular packing and higher crystallinity were observed in both neat films and blend films with NFA Y6-BO. Therefore, OSCs based on P4T-TCl achieved a higher PCE of 9.15%.[64]

2.2.3 Amide/alkyloxime-substituted polythiophenes. Incorporating amide functional groups is an alternative approach to achieve lower energy levels of PTs. In 2019, Zhou *et al.* reported a new strategy to downshift the HOMO energy levels of PTs by anchoring amide groups to bithiophene.[65] Two resulting amide-functionalized PTs exhibited deeper HOMO energy levels (∼−5.3 eV), leading to a higher V_{oc} (∼0.87 V) compared to P3HT (∼0.52 V). However, the 44BT:ITIC-based OSC showed a limited PCE of 0.85%, which is primarily due to the excessive phase separation caused by the poor solubility of 44BT. In 2020, the same group further introduced alkyloxime (–C(R′)=N–OR) into the PT backbone and reported two new PTs (PTOBT-*Z* with 93% of *Z*-isomer side chains and PTOBT-*Z*/*E* with mixed *Z*- and *E*-isomers at a ratio of 30 : 70). Both PTs exhibited deep-lying HOMO energy levels of approximately −5.44 eV. Benefiting from the more favorable blend morphology, a higher PCE of 9.04% was achieved for PTOBT-*Z*-based device.[66]

2.2.4 Cyano-substituted polythiophenes. As a commonly used strong electron-withdrawing group, the cyano group can significantly reduce the energy levels of PTs and improve the device performance.[67–70] In 2022, our group incorporated 3-cyanothiophene (CT) into the PT backbone and synthesized a new PT with an abbreviation of P5TCN-2F.[71] The cyano group endowed P5TCN-2F with a deep-lying HOMO energy level of −5.54 eV, leading to an increased V_{oc} (0.85 V) and reduced E_{loss} (0.53 eV) in OSCs. When paired with Y-series acceptors such as Y6, a new record PCE of 16.1% was achieved, marking a significant improvement over prior PT-based OSCs. Subsequently, we further developed a series of PTs (P5TCN-F*x*) with varying fluorination degrees to delicately control the polymer crystallinity and miscibility with Y6.[35] The backbone fluorination leads to strong interchain interaction, improved crystallinity, and appropriate thermodynamic miscibility with Y6. As a result, a prominent PCE of 17.2% was obtained using P5TCN-F25, setting a new efficiency record at the time and marking a big breakthrough for PT-based OSCs. Most recently, we achieved precise fibril network morphology control in the blend of P5TCN-HD (previously named P5TCN-F0) and eC9-2Cl through solubility-mediated nucleation regulation. This breakthrough yielded an unprecedented PCE of 18.12% with an FF of 79.17%, signifying a new breakthrough for PT-based OSCs.[72]

2.3 Design of PT derivatives

To finely tune the energy levels and aggregation behavior of PTs, polythiophene derivatives were widely developed. By classifying conjugated rings and linking bonds, we divide PT derivatives into poly(thiophene vinylenes) (PTVs) and heteroatom-substituted polythiophene analogs.

2.3.1 Poly(thiophene vinylenes) (PTVs). Poly(thiophene vinylene) (PTV) and its derivatives, consisting of alternating thiophene and vinylene units, offer distinct advantages as donor materials due to their structural simplicity and straightforward synthesis.[73,74] The vinylene linkers facilitate intramolecular and intermolecular hydrogen bonding, enhancing molecular planarity and promoting pre-aggregation in solution. These characteristics endow PTVs with higher hole mobility and red-shifted absorption spectra, making them particularly promising for OSC applications.[76–78]

In 2020, Bi *et al.* reported a series of PTVs with different alkyl side chains (Fig. 5).[78] Due to the random ester substituted positions, PTV:NFA-based OSCs all exhibited extremely low FFs (<40%) and PCEs (<3%). To investigate the influence of regioregularity on photovoltaic properties of PTVs, they developed a regioregular counterpart PTVT-C12, by copolymerizing alkyl ester-substituted thiophene–vinylene–thiophene (TVT) monomers and (*E*)-1,2-bis(trimethylstannyl)ethene (V–Sn). The improved regioregularity of PTVT-C12 was achieved by the locked direction of alkyl ester side chains on the TVT unit. Compared to its irregular counterpart PTV-C12, PTVT-C12 exhibited enhanced molecular ordering and higher hole mobility (2.17×10^{-4} cm^2 V^{-1} s^{-1}) in the film state, leading to an improved PCE of 6.44% in the resulting OSCs (Table 2).

In 2021, Ren *et al.* reported an ester substituted PTV derivative, PTVT-T, by inserting a thienyl bridge between every two alkyl ester-substituted TVT units.[26] The ester groups on the thiophene units endowed PTVT-T with a planar and stable conformation. When paired with three representative acceptors ($PC_{71}BM$, IT-4F, and BTP-eC9), the OSCs based on PTVT-T

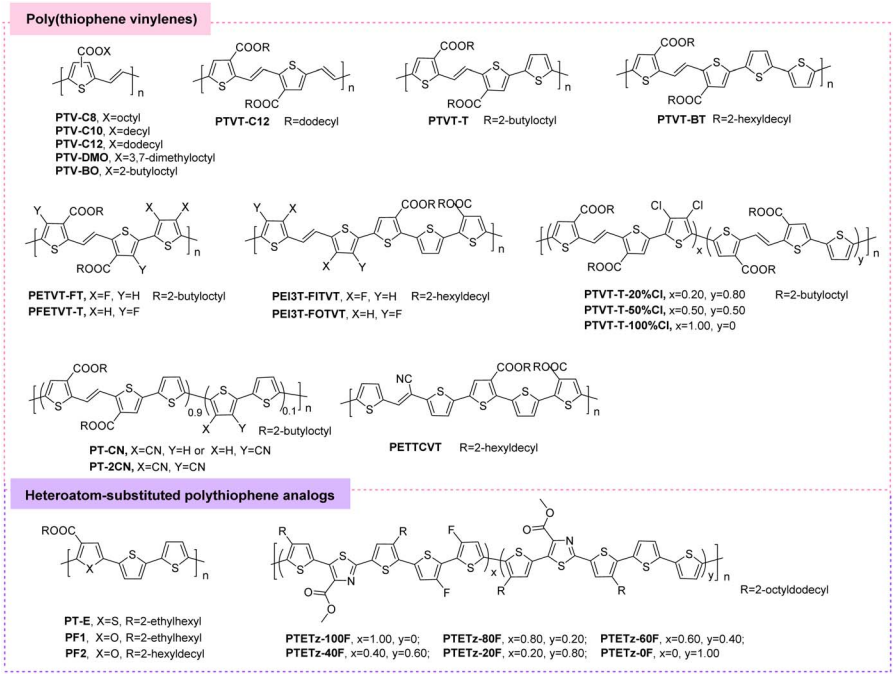

Fig. 5 The chemical structures of polythiophene derivatives.

achieved impressive PCEs of 7.25%, 11.28%, and 16.20%, respectively. With a material-only cost (MOC) of 35.0 $ per g, PTVT-T represents one of the most cost-effective high-performance polymer donors, highlighting its commercial potential. When paired with the non-fused acceptor GS60, the PTVT-T-based OSC achieved a PCE of 14.1%, which was a record value for OSCs containing fully non-fused donor–acceptor combinations at that time.[79] To further enhance both the efficiency and stability of PTV-based OSCs, Liu *et al.* introduced benzothiophene (BT) as a volatile solid additive. The low

Table 2 Energy levels and photovoltaic parameters of polythiophene derivatives

Polymer	HOMO/LUMO (eV)	Acceptor	V_{oc} (V)	J_{sc} (mA cm^{-2})	FF	PCE (%)	Ref.
PTV-C12	−5.30/−3.13	BO-4Cl	0.77	9.47	37.45	2.75	78
PTVT-C12	−5.31/−3.10	BO-4Cl	0.77	17.41	48.20	6.44	78
PTVT-T	−5.28/−3.02	BTP-eC9	0.79	26.22	78.0	16.20	26
PTVT-BT	−5.38/−3.02	BTP-eC9	0.79	26.75	77.14	16.31	81
PETVT-FT	−5.70/−3.09	L15	0.98	3.76	52.43	1.92	82
PFETVT-T	−5.63/−3.18	L15	0.93	19.74	64.33	11.81	82
PEI3T-FITVT	−5.41/−3.52	L8-BO	0.85	22.24	68	12.86	83
PEI3T-FOTVT	−5.44/−3.55	L8-BO	0.87	23.58	70	14.40	83
PTVT-20%Cl	−5.39/−3.05	A4T-16	0.85	20.7	67.4	11.8	84
PTVT-50%Cl	−5.42/−3.09	A4T-16	0.87	18.7	63.1	10.3	84
PTVT-100%Cl	−5.58/−3.07	A4T-16	0.98	10.2	56.1	5.58	84
PT-CN	−5.31/−2.95	BTP-eC9	0.81	27.67	77.0	17.27	36
PT-2CN	−5.32/−2.96	BTP-eC9	0.82	26.63	65.5	14.36	36
PETTCVT-L	−5.50/−3.71	L8-BO	0.91	18.95	56	9.65	85
PETTCVT-M	−5.41/−3.64	L8-BO	0.89	21.31	66	12.52	85
PETTCVT-H	−5.40/−3.64	L8-BO	0.88	23.53	74	15.32	85
PT-E	−5.21/−3.09	*m*-ITIC	0.82	13.07	59.8	6.41	86
PF1	−5.33/−3.10	*m*-ITIC	0.84	14.11	63.1	7.48	86
PF2	−5.37/−3.16	*m*-ITIC	0.87	17.17	73.5	10.98	86
		m-ITIC:$PC_{71}BM$	0.86	18.52	77.6	12.40	86
PTETz-0F	−5.29/−3.57	L8-BO	0.89	18.56	62.82	10.43	87
PTETz-20F	−5.30/−3.59	L8-BO	0.89	18.88	57.43	9.64	87
PTETz-40F	−5.31/−3.63	L8-BO	0.89	18.12	71.02	11.44	87
PTETz-60F	−5.33/−3.66	L8-BO	0.89	19.96	70.90	12.54	87
PTETz-80F	−5.37/−3.68	L8-BO	0.90	19.47	72.72	12.69	87
PTETz-100F	−5.39/−3.71	L8-BO	0.92	18.37	68.85	11.59	87

sublimation temperature of BT ensured its complete removal during spin-coating, eliminating the need for high-temperature annealing. As a result, the OSCs based on PTVT-T achieved an impressive PCE of 17.75%.[80]

In 2022, Bi *et al.* reported a high-performance polymer donor PTVT-BT by the copolymerization of a TVT unit with a bithiophene unit. Compared with PTVT-V, PTVT-BT showed much higher quantum efficiency of electroluminescence (EQE_{EL}, 7×10^{-3}%) and hole mobility (1×10^{-2} cm^2 V^{-1} s^{-1}), which facilitated efficient charge generation, transport, and collection. The OSC based on PTVT-BT showed a PCE of 16.31% without any processing additives. Furthermore, under indoor lighting conditions (2700 K LED, 1000 lux), the indoor OSC based on PTVT-BT:BTA3 attained a remarkable PCE exceeding 27%. Additionally, the tandem device with PTVT-BT as the donor of the sub-cell reached a PCE of 18.49%.[81] In 2023, Ma *et al.* reported a series of fully non-fused electron acceptors with different polar functional substituents to modulate the miscibility between PTVT-BT and the acceptor. Benefiting from the suitable phase separation, a PCE of 15.9% and a superior FF of 0.795 were achieved in the corresponding OSC.[88]

To optimize the photovoltaic performance of PTVs, An *et al.* reported a new TVT unit, FETVT, featuring vinyl-bridged fluorine and ester-substituted monothiophene. Incorporation of FETVT into the polymer backbone yielded PFETVT-T with a deep-lying HOMO energy level (−5.63 eV), suitable solution pre-aggregation, finely tuned polymer crystallinity, and appropriate thermodynamic miscibility with polymer acceptor L15. As a result, the OSCs based on PFETVT-T achieved a PCE of 11.81% in a PFETVT-T:L15-based binary device and 16.2% in a PM6:PFETVT-T:L15-based ternary device, demonstrating the significant potential of PTV materials for optoelectronic applications.[82] In 2024, Phan *et al.* developed two regio-isomeric fluorinated PTVs, PEI3T-FITVT and PEI3T-FOTVT, for constructing high-performance PTV-based OSC. PEI3T-FOTVT, which positioned the fluorine atoms on the "outside" of the TVT unit and exhibited enhanced backbone planarity through intramolecular F···S interactions, yielding enhanced aggregation and crystallinity. This molecular design strategy resulted in a 2.5-fold increase in hole mobility (from 1.4×10^{-4} to 3.6×10^{-4} cm^2 V^{-1} s^{-1}) and a corresponding PCE improvement, rising from 12.9% for PEI3T-FITVT to 14.4% for PEI3T-FOTVT.[83]

Alternative approaches to fluorination, such as chlorination and cyanation, provide more cost-effective and synthetically accessible routes. In 2023, Li *et al.* developed a series of chlorinated PTV donors (PTVT-T-*x*Cl, $x = 20\%$, 50%, 100%) through controlled chlorine substitution. The incorporation of chlorine effectively lowered the HOMO energy levels (≤−5.3 eV) and modulated polymer crystallinity. Consequently, the OSC based on PTVT-T-20%Cl achieved the highest PCE of 11.8%, which is attributed to the more moderate nanoscale phase separation.[84] In 2024, Ai *et al.* developed two ternary PT donors, PT-CN and PT-2CN, by inserting one or two cyano groups into PTVT-T. The introduction of cyano groups not only downshifted the HOMO energy levels, but also reduced the miscibility of the PTs with the acceptor BTP-eC9. Among them, PT-CN well balanced the multiple impacts to obtain the finest morphology with the highest crystallinity. As a result, the OSC based on PT-CN achieved an impressive PCE of 17.27%, accompanied by the best J_{sc} of 27.67 mA cm^{-2} and FF of 77.0%.[36]

To simultaneously enhance the PCE and stretchability of PTV-based OSCs, in 2023, Lee *et al.* introduced a cyanovinylene unit into PTV-based polymer and developed a new PTV (PETTCVT-X, X = L, M, and H) with tuned molecular weight (M_n = 14.6–39.2 kg mol^{-1}). The crystallinity of the PTVs increased progressively with an increase in M_n, leading to enhanced hole mobility and suppressed charge recombination in the OSCs. Moreover, both the mechanical stretchability and electrical properties of the PTVs improved significantly with the increasing M_n, which was ascribed to the formation of tie-chains that connect the isolated crystalline domains. Consequently, the OSC featuring PETTCVT-H with the highest M_n exhibited the highest PCE of 15.3% and a crack-onset strain (COS) of 7.1%, significantly outperforming its lower-M_n counterparts (PETTCVT-L:PCE = 9.7%, COS = 1.3%; PETTCVT-M:PCE = 12.5%, COS = 3.7%). Notably, the intrinsically stretchable (IS)-OSCs utilizing PETTCVT-H maintained 80% of their initial efficiency ($PCE_{80\%}$ = 10.1%) even at a strain of 16%.[85]

2.3.2 Heteroatom-substituted polythiophene analogs. As analogs of thiophene, furan and its derivatives feature higher electronegativity, smaller volume, larger dipole moment, and lower Dewar resonance energy.[89,90] Moreover, furan and its derivatives are indisputably sustainable owing to their biodegradable and biorenewable properties.[91–93] In 2022, Gao *et al.* developed two novel furan-based PT derivatives (PF1 and PF2) by incorporating an alternating furan-3-carboxylate and 2,2′-bithiophene unit. Compared to their all-thiophene counterpart PT-E, PF1 and PF2 showed higher hole mobilities, larger dielectric constants, and deeper HOMO energy levels (≤−5.33 eV). The improved physicochemical properties of PF1 and PF2 resulted in PCEs of 7.48% and 10.98%, respectively, representing enhancements of approximately 16.7% and 71.3% compared to PT-E-based devices (6.41%). Notably, the optimized devices based on PF2:*m*-ITIC:$PC_{71}BM$ achieved a higher efficiency of 12.40%.[86]

Thiazole (Tz) is a low-cost building block, where the nitrogen atom can generate intramolecular N···S noncovalent conformational locks, ensuring good backbone planarity for effective charge transport.[94–96] Capitalizing on this feature, Wang *et al.* developed ester-functionalized thiazole (E-Tz) as an electron-withdrawing unit for designing efficient PT derivatives (PTETz-*x*F, x = 100, 80, 60, 40, 20 or 0). PTETz-80F exhibited suitable temperature-dependent aggregation and compact molecular packing, which significantly enhanced exciton dissociation probability and charge collection efficiency in the resulting OSC, yielding a higher PCE of 12.69%.[87]

3. Morphology control and device engineering of PT:NFA blends

It is well known that the active layer morphology has a profound impact on the photovoltaic performance of OSCs by governing

charge generation and transport processes.[97–99] For PT-based OSCs, the PCE is largely limited due to the difficulty in morphology optimization. The non-fused conjugated backbones of PTs induce twisting in their main chains, which results in weak preaggregation in solution and hyper-miscibility with NFAs in the film state. Therefore, precise control of active layer morphology represents a key strategy for developing high-performance PT solar cells. This section will provide a detailed discussion of morphology control methods for PT-based OSCs.

3.1 Miscibility matching between PT and NFAs

From the perspective of thermodynamics, the formation of morphology and the purity of mixed domains are governed by molecular interactions, which are determined by the thermodynamic Flory–Huggins interaction parameter (χ).[100,101] A lower χ corresponds to higher donor–acceptor miscibility, which should lead to a mixed amorphous phase. Conversely, a higher χ value tends to promote the formation of relatively purer phases with limited intermixing. In this section, we will present a comprehensive review of miscibility matching rules in PT-based OSCs from the aspects of molecular engineering, acceptor matching and additives.

3.1.1 Molecular engineering. To match well with prevailing NFAs, rational molecular optimization of polymer donors is highly desirable. Given that the backbone of polythiophenes is composed entirely of thiophene units, rational functionalization of PTs is essential for modulating their properties. In 2021, Xiao *et al.* reported that the fluorinated polythiophene P4T2F-HD shows moderate miscibility with prevailing NFA, Y6-BO, whereas the P3HT:Y6-BO system demonstrates much higher miscibility. Consequently, the P4T2F-HD:Y6-BO blends formed a desirable phase-separated morphology in PT-based OSCs (PCE = 13.65%), which contrasts with the completely mixed film morphology observed in the low-efficiency P3HT:Y6-BO blend, which exhibited a PCE of only 0.38%.[54] The crucial effect of fluorination on miscibility control was also confirmed in the research of Yang *et al.*,[57] Li *et al.*,[102] He *et al.*,[103] and Jeong *et al.*[58] In 2023, our group investigated the effect of varying fluorination degrees in PTs on miscibility with acceptors and blend morphologies.[35] We found that the PTs (P5TCN-F*x*) with higher fluorination degrees exhibited decreased miscibility with Y6 (Fig. 6a). The P5TCN-F0:Y6 blend exhibited the best miscibility, but the hyper-solubility of P5TCN-F0 caused the largest surface roughness and excessive phase separation in the blend film, which was identified as the primary reason for its poor photovoltaic performance (PCE = 11.5%). For P5TCN-F25 and P5TCN-F35 blends, moderate solubility and appropriate miscibility resulted in favorable morphologies with suitable phase separation, enabling the highest PCE exceeding 16% in the resulting OSCs. In contrast, P5TCN-F50:Y6 exhibited large phase separation due to lowest miscibility and solubility, leading to a decreased PCE of 14.6% for the OSC.

In addition to the degree of fluorination, An *et al.*[82] and Phan *et al.*[83] demonstrated that the fluorine substitution position on the PT/PTV backbone critically affects the miscibility with acceptors, thereby influencing blend morphology and photovoltaic performance. For instance, compared to PETVT-FT with two fluorine atoms located on the thiophene unit, its counterpart PFETVT-T, in which two fluorine atoms were located on the TVT unit, exhibited better miscibility with the polymer acceptor L15. These results led to a more evenly distributed nanofiber structure and a higher PCE of 11.81% in the devices.[82] Similarly, Phan *et al.* demonstrated that the "outside" location of fluorine atoms on the TVT unit in PEI3T-FOTVT leads to decreased miscibility with the acceptor L8-BO. The reduced miscibility promotes larger domain sizes and higher domain purity in the blend morphology, which facilitates faster charge transport and reduces recombination. Consequently, the PEI3T-FOTVT:L8-BO films achieved an improved PCE of 14.4% in OSCs.[83]

In addition to halogens, the use of other functional substituents, such as the cyano group, has emerged as an effective approach to modulate the miscibility of PT derivates. In 2023, our group investigated the differences in miscibility between non-cyano-substituted PT (P4T2F-HD) and cyano-substituted PT (P5TCN-2F) with different Y series acceptors. The best miscibility of P4T2F-HD:Y6 forced the blends to form completely mixed morphology with low domain purity, which resulted in inferior photovoltaic performance (PCE = 2.9%) in the resulting OSC. For the P4T2F-HD:Y6-BO blend, decreased miscibility indicated better phase separation, which can facilitate charge transport and improve their device performance (PCE = 13.6%). For P5TCN-2F blends, further decreased miscibility resulted in enhanced phase separation and interpenetrating networks, thus leading to improved PCE (15.8–16.1%) in the resulting OSCs.[71] Similar miscibility matching rules have also been observed in the PTV:NFA system. In 2024, Ai *et al.* revealed that cyanation of the molecular backbone promotes de-mixing of PTs and the acceptor (BTP-eC9). The introduction of 3-cyanothiophene (3-CT)/3,4-dicyanothiophene (DCT) units monotonically reduced the miscibility with BTP-eC9, which is consistent with the improved phase separation. Moderate miscibility in PT-CN:BTP-eC9 resulted in proper phase separation and ordered molecular stacking, enabling efficient exciton dissociation and low trap density. Consequently, PT-CN-based OSCs achieved the highest charge mobilities and longest charge lifetimes, leading to the highest PCE of 17.27%.[36]

Side chains play a considerable role not only in improving the solubility of polymers for solution-processed device fabrication,[104,105] but also in affecting the molecular packing, miscibility with the acceptor and the device performance.[106,107] In 2021, Liu *et al.* investigated the influence of the side chain length of poly(3-alkylthiophene) on its miscibility with an acceptor (ZY-4Cl) and the blend morphology. They revealed that compared with poly(3-alkylthiophene) with even carbon chains, poly(3-alkylthiophene) with odd carbon chains exhibited decreased miscibility with ZY-4Cl. Moreover, as the carbon chain lengthened, a gradual increase in miscibility between the polymer and ZY-4Cl was observed. Finally, P3PT demonstrated a more ideal phase separation morphology, resulting in balanced molecular packing and achieving a superior PCE of 9.75% in OSCs.[42] Guided by theoretical calculations of interaction parameters, Wang *et al.* systematically adjusted the

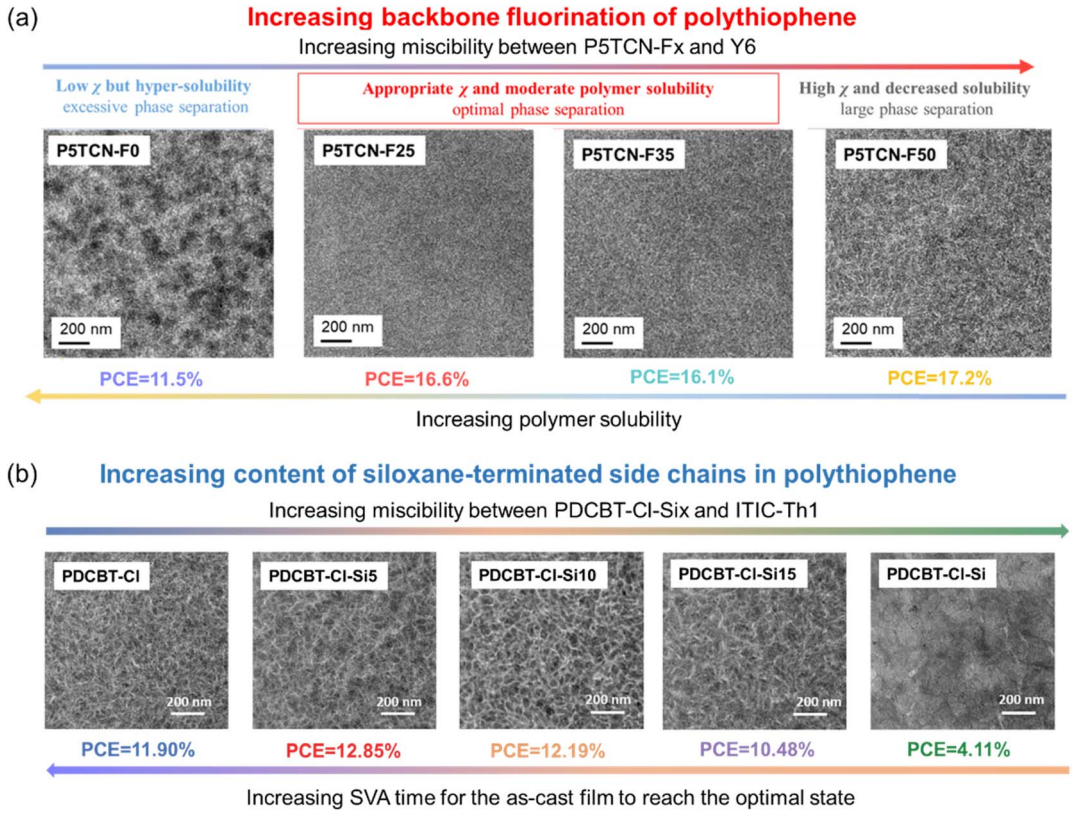

Fig. 6 (a) The miscibility-blend morphology-device performance relations in P5TCN-*Fx*:Y6 blend systems.[35] (b) The miscibility-blend morphology-device performance relations in PDCBT-Cl-Six:ITIC-Th1 blend systems.[63]

miscibility of PDCBT-Cl:ITIC-Th1 blends by varying the proportion of siloxane-terminated chains in PTs (Fig. 6b) and revealed that the miscibility between PT and ITIC-Th1 gradually decreases with the increasing content of siloxane-terminated chains. For blends with low miscibility, the mixed phase composition in the as-cast film approached the percolation threshold rapidly, indicating a shorter solvent vapor annealing (SVA) time for device optimization. By methodically altering the percentage of siloxane-terminated units, they found that the OSCs based on PDCBT-Cl-Si5 achieved the highest PCE of 12.85%, attributed to its slightly decreased miscibility, proper domain composition and the nano-scale interconnecting network.[63] Next, Zhang *et al.* analyzed the thermodynamic miscibility between an acceptor (BTP-eC9) and PTs with different aromatic rings as side chains. Compared with selenophene-based PT4F-Se, the thiophene substituted PT4F-Th exhibited decreased miscibility with BTP-eC9, which synergistically led to higher domain purity in the blend. As a result, a higher PCE of 16.4% was achieved in PT4F-Th-based OSCs.[46]

It has been well recognized that controlling the molecular weight of π-conjugated polymers is of significance for their aggregation behaviors or morphology within active layers.[68,108,109] For P3HT:NFA systems, Liu *et al.* demonstrated a strong molecular weight dependence in OSCs based on P3HT:ZY-4Cl. As the M_n varied from 6.0 to 35.9 kg mol^{-1}, the PCE ranged from 4.66% to 9.60%, with the highest efficiency achieved at M_n = 17.2 kg mol^{-1}. With the increasing M_n of P3HT, the miscibility between P3HT and ZY-4Cl gradually decreases. Morphological characterization revealed the P3HT with a medium M_n of 17.2 kg mol^{-1} showed the most favorable domain structure and the highest crystallinity, which led to the best PCE of 9.60% for its resulting OSCs.[41] For the system of P5TCN-F25:Y6, our group found that as the M_n of P5TCN-F25 increased from 30 to 57 kg mol^{-1}, the miscibility between P5TCN-F25 and Y6 exhibited a monotonically decreasing trend, which could be attributed to the reduction in mixing entropy due to the increasing chain length. When the M_n further increased to 73–89 kg mol^{-1}, the miscibility between P5TCN-F25 and Y6 slightly increased, which might be due to the dilution of immiscible groups on the main chain and end groups. Therefore, compared with P5TCN-F25 with medium M_n, more ideal phase separation can be achieved in OSCs based on P5TCN-F25 with high M_n, which is consistent with observed improvements in J_{sc} (26.8–26.9 mA cm^{-2}) and PCE (16.5–16.7%).[110]

3.1.2 Acceptor selection. The selection of suitable acceptors for OSCs is crucial for optimizing performance. Yang *et al.* identified excessive miscibility between P3HT and an A–DA′D–A-type NFA (BTP-4Cl) as the primary limitation, yielding fully mixed blends with poor PCE (~1%). By modifying the cyano-substituted end groups in BTP-4Cl, the new acceptor ZY-4Cl showed decreased miscibility with P3HT, which optimized the

phase separation morphology and achieved a record PCE of 9.46%.[111] Following this path, Gao *et al.* thoroughly investigated the thermodynamic miscibility of P3HT with a range of NFAs (A–DA′D–A-type: Y6 and ZY-4Cl; A–D–A type: ITIC and IDTBR) (Fig. 7a). The P3HT:ZY-4Cl pair showed the lowest miscibility among the four systems, leading to a more optimal blend morphology and the highest PCE of 10.2%. In contrast, P3HT exhibited the best miscibility with ITIC, resulting in inefficient charge transport and a poor PCE of 1.37%.[112] In the same year, our group conducted a study employing DCNBT-IDT, N2200 and PYT as polymer acceptors, with P3HT serving as the donor, to investigate the relationship between thermodynamic miscibility and phase separation morphology. The results revealed that N2200 and PYT were thermodynamically immiscible with P3HT, which led to excessive phase separation in blending films. Consequently, the devices based on P3HT:N2200 and P3HT:PYT exhibited relatively low PCEs of 1.50% and 1.65%, respectively. Notably, DCNBT-IDT showed appropriate thermodynamic miscibility with P3HT, leading to a well-mixed nanofiber phase-separated morphology. Encouragingly, the device based on P3HT:DCNBT-IDT achieved an unprecedented PCE of 7.35%, setting a new benchmark for P3HT-based all-polymer solar cells (all-PSCs).[113]

For PT:NFA systems, in early 2020, Liang *et al.* established critical structure-miscibility-device performance relationships for efficient PT (PDCBT-Cl):NFA (Y6, ITIC-Th1, ITIC, IDIC, or ITIC-Th) pairs. Through a detailed analysis of interaction parameters and domain purity, they discovered that the good miscibility between PDCBT-Cl and Y6 was the major reason for the poor PCE (0.5%) in OSCs (Fig. 7b). In contrast, the optimally miscible system (PDCBT-Cl:ITIC-Th1) afforded the best PCE of 12.11% with the highest J_{sc} (18.3 mA cm^{-2}) and FF (70.0%).[114]

Despite the profound understanding of PT:NFA, the development of all-PSCs based on PTs remains limited, with relatively few studies conducted. To address this issue, Ma *et al.* systematically studied the intermolecular interactions between PTs and polymer acceptors and established a clear correlation between the chemical structure and blend compatibility. Introducing an ester group in P3HT suppressed the interaction energy between the donor (PDCBT) and the acceptor (PY-IT), which was beneficial for suppressing the miscibility and obtaining desirable phase separation in the PDCBT:PY-IT blend. Consequently, the PDCBT:PY-IT combination exhibited more optimal phase separation with improved domain purity, achieving a remarkable PCE of 15.3% in the resulting all-PSCs.[115]

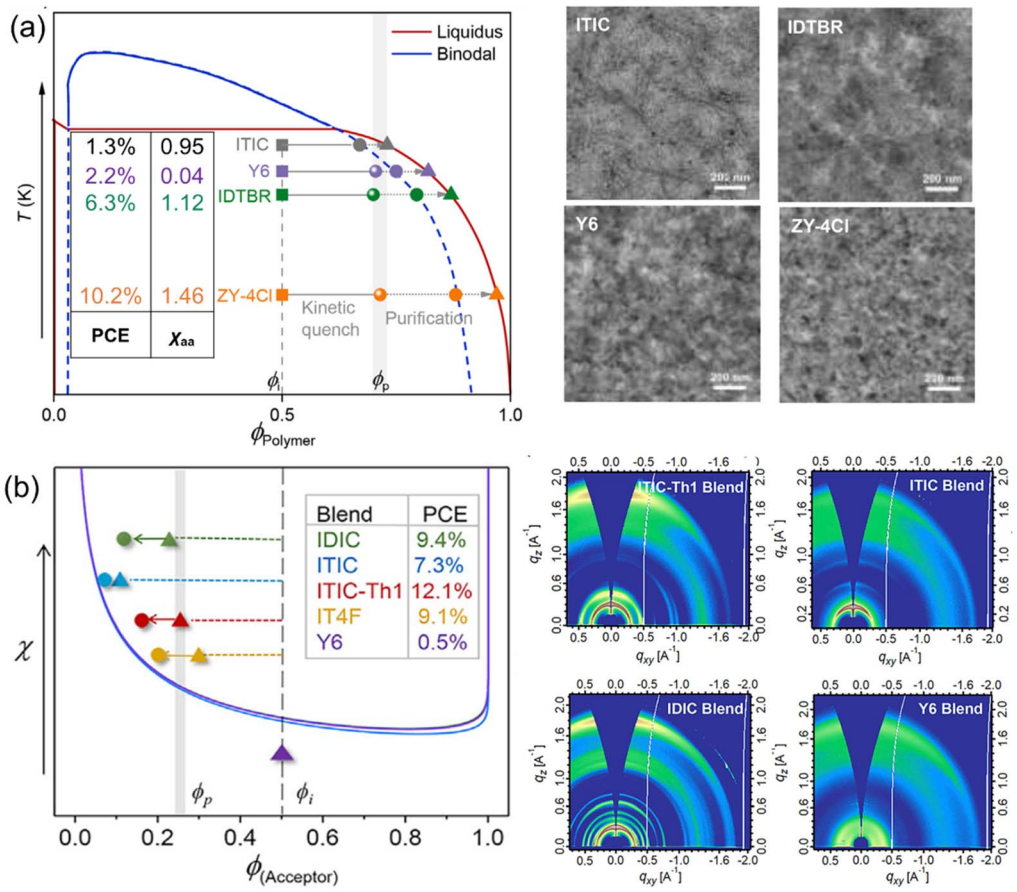

Fig. 7 (a) The schematic interaction parameter-composition phase diagram, optimal blend morphology and device performance of various P3HT:NFA blend systems.[112] (b) The schematic interaction parameter-composition phase diagram, molecular ordering, and device performance of various PDCBT-Cl:NFA blend systems.[114]

3.1.3 Additives. Strategic utilization of additives provides precise control over active layer morphology, serving as a powerful tool for optimizing the performance of OSCs.[116,117] In 2021, Yang *et al.* revealed that the solid additive (SA4) demonstrated high compatibility with the acceptor ZY-4Cl but poor compatibility with P3HT. Compared to the OSC treated with 1,8-diiodooctane (DIO), the OSC treated with SA4 exhibited more ideal phase separation and ordered molecular packing, thereby reducing the carrier recombination, enhancing charge generation and transport, and significantly improving the PCE to 10.24%.[118] In a recent study, Liu *et al.* introduced a new volatile solid additive, benzothiophene (BT), for enhancing the efficiency of PT-based OSCs (Fig. 8a). Thermodynamic miscibility analysis indicated that the addition of BT to PTVT-T:BTP-eC9 films significantly improved the donor/acceptor compatibility (Fig. 8b and c). Conversely, blends treated with benzodithiophene (BDT) or benzotrithiophene (BTT) exhibited reduced miscibility, leading to increased aggregation and phase separation. Consequently, the OSC treated with BT achieved a PCE of 17.75%, which is the highest value for PTV-based OSCs.[80]

3.2 Solution aggregation manipulation of PT

The aggregation behavior of conjugated polymers in solution significantly influences the crystallinity, phase purity, and phase separation of the resulting blend films, ultimately affecting the device efficiency. In this section, the impact of polythiophene solution aggregation structures on film morphology and strategies for modulating solution aggregation states are discussed.

In 2020, An *et al.* investigated the modulation of solution aggregation behavior and film morphology in P3HT-based OSCs by utilizing non-halogenated solvents.[119] By replacing the traditional halogenated solvent chlorobenzene (CB) with 2-methylanisole (*o*-MA) and the incorporation of 1-methylnaphthalene (1-MN) as an additive, the pre-aggregation of P3HT in solution was significantly enhanced. Morphological characterization revealed that blend films processed with *o*-MA exhibited large-scale nanofibrous structures, which starkly contrasted with the fiberless morphologies observed in CB-processed films. As a result, the P3HT-based OSC fabricated with *o*-MA achieved a PCE of 7.1% for small-area devices (0.05 cm^2) and maintained a PCE of 6.89% for large-area devices (1 cm^2).

To unravel the deep correlations between solution aggregation behavior, device performance, and thermal stability, Gao *et al.* directly quantified the solution structure of PT:NFA blends for the first time (Fig. 9a and b).[120] Small-angle neutron scattering (SANS) results revealed that the rigidity of the aggregates in low molecular ordered polymer blend solutions (PM6:Y6) decreased compared to their polymer solutions. In contrast, higher molecular ordered polymers, such as P3HT and P5TCN (previously named P5TCN-2F), exhibited enhanced rigidity and increased cross-sectional area of the solution aggregates, leading to higher crystallinity in the blend films. Consequently, the highly molecular ordered P5TCN:Y6 system achieved ordered aggregation in blend solutions, which was inherited in the films, thereby affording the best PCE of 16.1% and excellent thermal stability (the estimated 80% of the initial PCE, T_{80} = 1100 hours) for polythiophene solar cells. Following this path, Gao *et al.* investigated the temperature-dependent aggregation behaviors of PT derivatives (PTVT-T) and fused-ring polymers (PBQx-TF and PM6) in NFA systems.[121] For the PTVT-T blend system, an increase in solution temperatures led to the disaggregation of initial large-scale polymer clusters, resulting in a notable increase in Kuhn length (L_1). Higher temperatures facilitated the crossing of the energy potential barrier by the polymer chains, leading to an improved acceptor distribution ratio (Φ), enhanced the relative degree of crystallinity (rDoC) and reduced phase size in films (Fig. 9c). Finally, the PCE of OSCs based on PTVT-T increased monotonically from 11.5% to 15.5% (Fig. 9d). Conversely, the PBQx-TF blend exhibited exceptional temperature resilience. Despite increasing solution

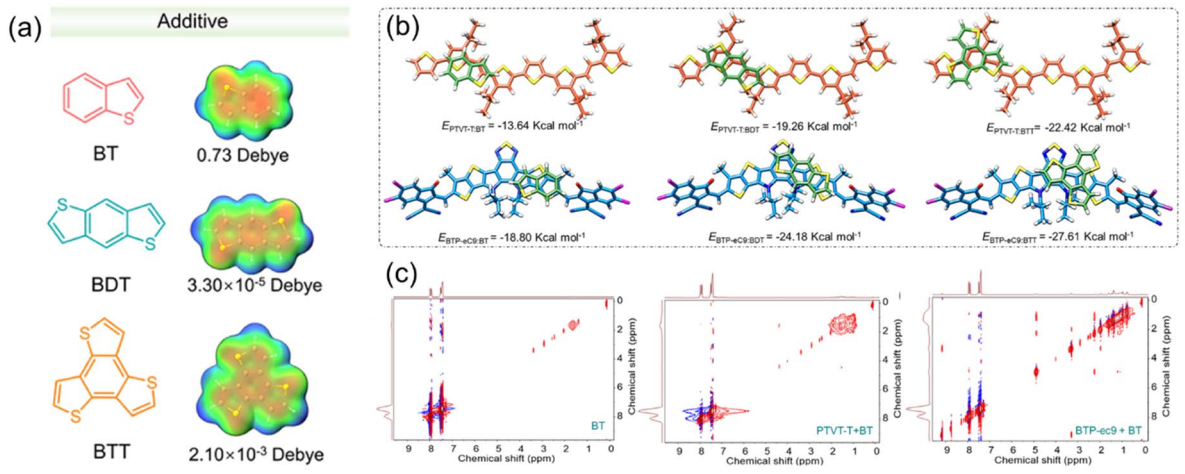

Fig. 8 (a) Molecular structures and electrostatic potential (ESP) profiles of additives (BT, BDT and BTT). (b) The most stable conformations and estimated binding energies for the complexes of PTVT-T:BT, BTP-eC9:BT, PTVT-T:BDT, BTP-eC9:BDT, PTVT-T:BTT, and BTP-eC9:BTT. (c) 2D ^1H–^1H nuclear Overhauser effect spectroscopy (NOESY) spectra of BT, PTVT-T + BT, and BTP-eC9 + BT.[80]

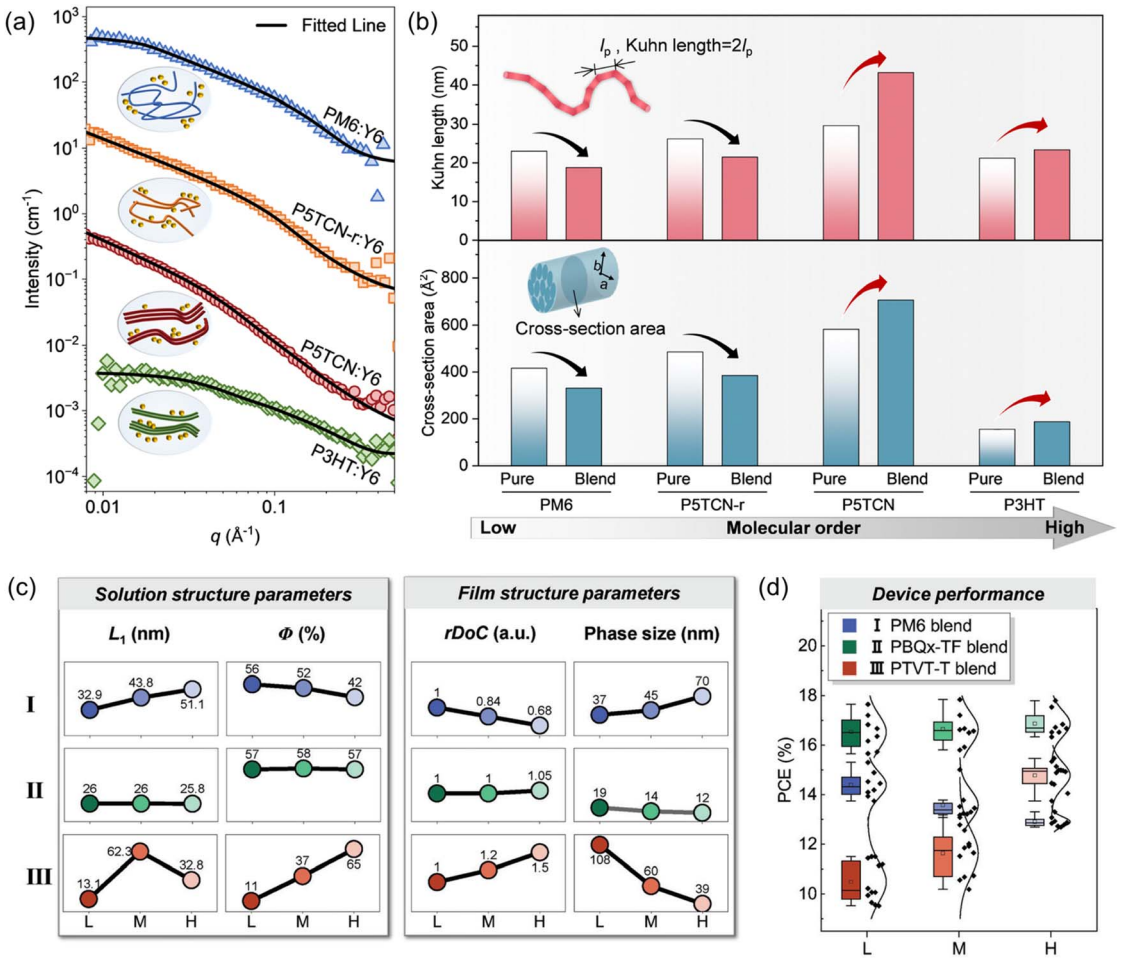

Fig. 9 (a) The small-angle neutron scattering (SANS) curves of four polymer solutions. (b) The Kuhn lengths and the cross-section areas of the aggregate fibers of the four polymer solutions and the corresponding blend solutions.[123] (c) Plots of the variation of solution-state structure parameters and film structure parameters with solution temperature for binary organic photovoltaic systems based on PM6, PBQx-TF and PTVT-T; (d) PCE evolution with elevated solution temperature for the PM6 blend (blue), PBQx-TF blend (green), and PTVT-T (red) binary blends.[121]

temperatures, it maintained well-organized aggregated fiber structures ($L_1 \approx 26$ nm, $\Phi \approx 58\%$) and stable crystalline behavior in the films (rDoC $\approx$ 1), yielding consistent device performance (PCE $\approx$ 17.8%) regardless of the solution temperature. For the PM6 blend system, as the temperature increased, the blend film exhibited reduced rDoC and intensified phase separation, which was ascribed to the loose polymer aggregates in solution with high temperature. Consequently, the reduced crystallinity and coarser phase separation resulted in a decline in PCE (from 15.3% to 13.3%) at elevated solution temperature.

As the fabrication of highly efficient polythiophene solar cells still heavily relies on halogenated solvents and additives, which pose significant risks to both the environment and human health, processing with eco-friendly non-halogenated solvents would significantly benefit the industrial manufacturing and practical application of OSCs. To improve the efficiency of PT solar cells *via* non-halogen processing, our group investigated the temperature-dependent aggregation effects of PT in *o*-xylene (*o*-XY) on film morphology. As the processing temperature increased, both donor (P5TCN-F25) and acceptor (Y6-BO) molecules exhibited enhanced face-on orientation and reduced aggregation in the blend films, leading to improved charge transport in the resulting PT-based OSCs. Transmission electron microscopy (TEM) analysis indicated that the films processed at 100 °C developed an optimal bicontinuous interpenetrating network morphology with a well-dispersed fibrillar structure, which enhanced both charge generation and transport, thus resulting in a higher PCE of 15.64% in OSCs. However, when the processing temperature further increased to 130 °C, the blend morphology became excessively mixed, leading to decreased phase separation and increased charge recombination, which ultimately reduced the PCE to 14.53%.[122]

To further finely manipulate polymer aggregation in solution and optimize fibrillar morphology in films with eco-friendly solvents, our group recently reported a strategy for precisely regulating the nucleation driving force of polythiophene (P5TCN-HD) based on Classical Nucleation Theory (CNT) (Fig. 10a).[72] As shown in Fig. 10b, P5TCN-HD exhibited lower

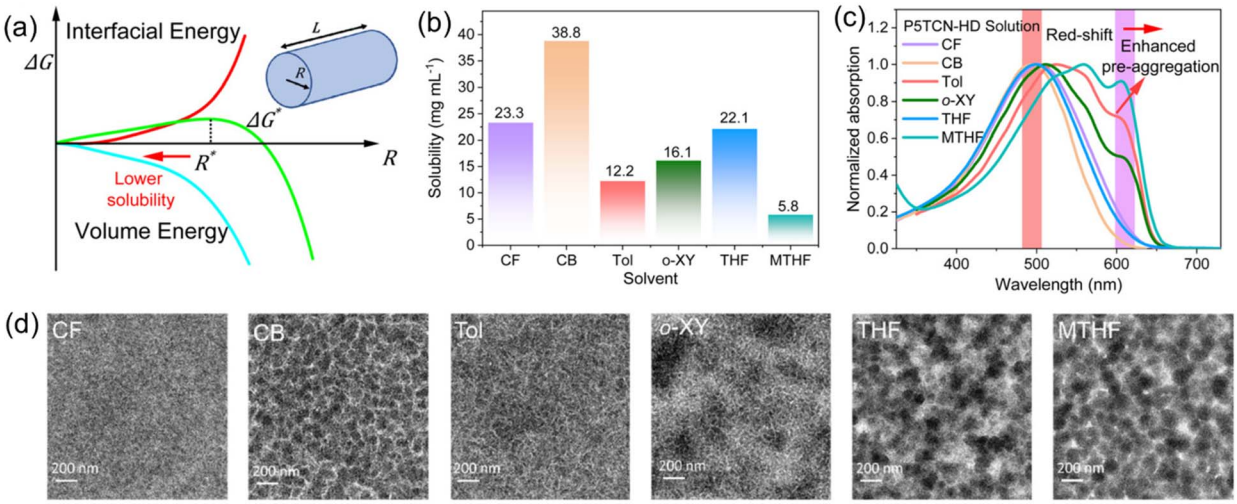

Fig. 10 (a) Schematic representation showing the dependence of Gibbs free energy of nucleation (ΔG^*) on the radius R according to classical nucleation theory; (b) the solubility of P5TCN-HD in different solvents; (c) normalized absorption spectra of P5TCN-HD in varied solvents. (d) Transmission electron microscopy (TEM) images of the blend films processed with different solvents.[72]

solubility in non-halogenated solvents, including toluene (Tol, 12.2 mg mL^{-1}), *o*-xylene (*o*-XY, 16.1 mg mL^{-1}), and 2-methyltetrahydrofuran (MTHF, 5.8 mg mL^{-1}), compared to halogenated solvents such as chloroform (CF, 23.3 mg mL^{-1}) and chlorobenzene (CB, 38.8 mg mL^{-1}). The reduced solubility enhanced solution pre-aggregation (Fig. 10c), thereby facilitating nucleation and fibril growth. When processed with CF, the P5TCN-HD:eC9-2Cl blend films exhibited a homogeneous morphology without distinct fibrillar structures (Fig. 10d). In contrast, films processed with Tol and *o*-XY displayed well-defined fibrillar networks, while those processed with MTHF exhibited excessive phase separation with particle-like domains. The refined fibrillar network in Tol-processed films significantly enhanced the PCE to 17.10%, which was notably higher than those processed with CF (14.49%) and MTHF (8.91%).

3.3 Modulation of the film-formation process

To further improve the morphological control of PT:NFA blend films, modulating the film-forming process is an effective strategy in addition to regulating polymer aggregation behavior in solution.[124] In 2019, Liang *et al.* reported a cosolvent strategy involving CB with 1,2,4-trichlorobenzene (TCB) to separate the crystallization of P3HT and the acceptor (O-IDTBR), thereby extending the film-forming duration (Fig. 11a). In the CB:TCB solvent system, the prior crystallization of P3HT induced solid–liquid phase separation, facilitating the formation of a nano-interpenetrating network. For the solution without TCB, both P3HT and O-IDTBR crystallized simultaneously, making it challenging to achieve distinct P3HT and O-IDTBR phases. Consequently, a highly crystalline nano-interpenetrating network with proper vertical phase separation was obtained in CB:TCB processed blend films, boosting the PCE from 4.45% to 7.18% in the resulting OSCs.[125]

In order to further investigate the effects of the cosolvent characteristics on film-forming kinetics and film morphology, Liu *et al.* categorized cosolvents into three groups based on their boiling points relative to the host solvent CB. Cosolvents with lower boiling points, such as CF, can facilitate a faster film-forming process. The introduction of CF reduced crystallinity for both components, leading to a relatively low PCE of 4.24% in the resulting OSCs. In contrast, cosolvents with higher boiling points, such as *o*-dichlorobenzene (*o*-DCB) and TCB, enable a more extended self-organization process for P3HT and O-IDTBR. This separation and prolongation of the crystallization process facilitate the formation of a highly crystalline nano-interpenetrating network, which significantly enhances device performance. As a result, OSCs processed with TCB or *o*-DCB achieved PCEs of 7.20% and 7.09%, respectively. However, the use of cosolvents with very high boiling points, such as chlornaphthalene (CN), resulted in residues within the film that maintained self-organization of P3HT and O-IDTBR for extended periods. This prolonged self-organization led to increased phase separation, ultimately resulting in a lower PCE of 5.32%.[126]

To further monitor the evolution of PT:NFA structures from solution to film, in 2022, Jeong *et al.* analyzed the *in situ* UV-Vis absorption spectra of blends based on two PTs with different numbers of fluorine atoms on their backbone. The morphology of the PT-4F:BTP-eC9 blend was quenched within 0.57 s during film formation, significantly faster than PT-2F:BTP-eC9 (0.89 s). This rapid solidification was attributed to the more strongly pre-aggregated state of PT-4F in solution. Rapid solidification restricted liquid–liquid phase separation, leading to a kinetically quenched/intermixed blend morphology. As a result, PT-4F leads to the formation of a morphology with large donor–acceptor interfaces and well-developed crystalline domains, which ultimately led to an increased PCE of 15.6% in the resulting OSCs.[58]

To unravel the deep correlations between solution effects, blend morphology and device performance, our group

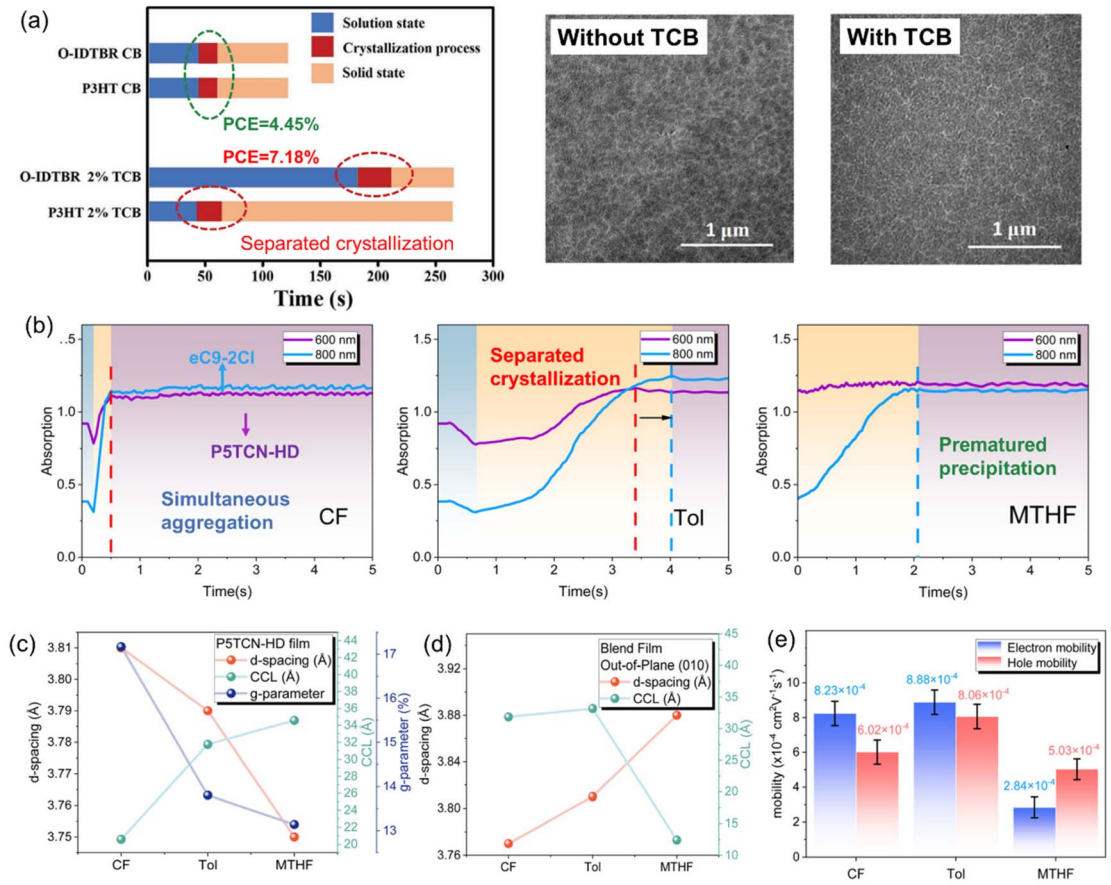

Fig. 11 (a) Schematic illustration of time scales of the film-forming process of P3HT:O-IDTBR blends without or with TCB.[125] (b) Line-cut at 600 (purple, P5TCN-HD) and 800 nm (blue, eC9-2Cl) wavelengths of *in situ* UV-vis absorption spectra for P5TCN-HD:eC9-2Cl blend solutions in different solvents. (c and d) *d*-Spacing and crystal coherence lengths (CCLs) of the (010) diffraction peak and paracrystalline disorder (*g*-parameter) of the P5TCN-HD neat (c) and blend films (d). (e) Hole and electron mobilities of the solar cells based on P5TCN-HD:eC9-2Cl processed with different solvents.[72]

investigated the spin-coating process of the P5TCN-HD:eC9-2Cl blend using different solvents. The lower volatility of Tol extended the film drying time (Fig. 11b), facilitating the initial formation of a gel-like fibrillar framework by P5TCN-HD, followed by controlled crystallization of the acceptor eC9-2Cl within the network. This process ultimately resulted in a bicontinuous fibrillar morphology, leading to the highest PCE of 17.10% in the resulting OSC. Conversely, the rapid drying of solvent CF maintained the well-mixed state of the donor and acceptor from solution to solid films, resulting in a blend with small phase domains and numerous interfaces (Fig. 11c and d). However, the extremely low solubility of MTHF triggered excessive crystallization of the acceptor, leading to large phase-separated domains (102.3 nm) that hindered charge transport and caused a poor PCE of 8.91% (Fig. 11e).[72]

3.4 PT-based all-polymer OSCs

All-polymer solar cells (all-PSCs) based on P3HT offer several advantages for industrial-scale production, including low cost, excellent stability, and mechanical flexibility.[127,128] However, the wide bandgap of P3HT (~1.9 eV) poses a limitation for near-infrared absorption. Additionally, the challenging morphology control with polymer acceptors impedes the efficient charge transfer. As a result, there has been limited progress in PCE over the years. To address this challenge, recent research has concentrated on developing novel polymer acceptors specifically designed to pair with P3HT for enhancing device performance.[129–131]

Among the various available electron-withdrawing units, imide functionalized arenes are favored building blocks for electron transport materials due to their high electron affinity and solution-processing properties.[132,133] The polymer N2200, composed of naphthalenediimide (NDI) and thiophene units, stands out as a preeminent representative of polymer acceptors for organic field-effect transistors (OFETs) and OSCs.[134–136] However, the research by Ohkita *et al.*[137] and Nakamura *et al.*[138] showed that P3HT:N2200 blend films exhibited remarkably low J_{sc} (<1.5 mAcm^{-2}) and PCE (<1%), which was mainly ascribed to the formation of extensive phase-separated domains (>100 nm).

The polymer DCNBT-IDT, copolymerized from indacenodithiophene (IDT) and cyano-substituted benzothiadiazole (BT) units, is an ideal polymer acceptor for P3HT-based all-PSCs owing to its favorable energy levels and short-range ordered

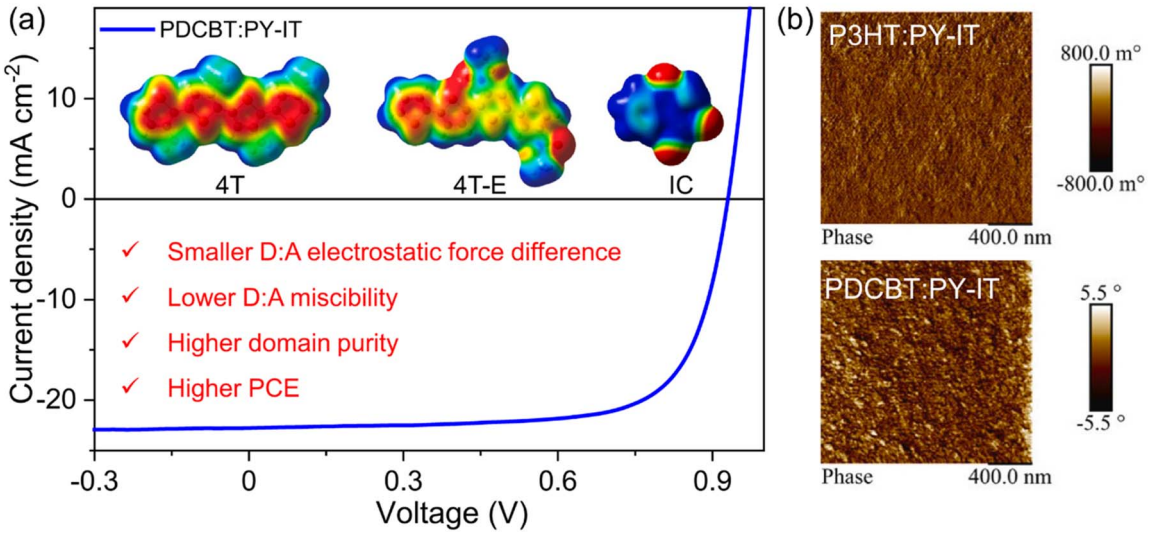

Fig. 12 (a) The electrostatic potential (ESP) distributions and device performance of PDCBT. (b) Atomic force microscopy (AFM) phase images of the P3HT:PY-IT and PDCBT:PY-IT blend films.[115]

microstructure.[139] In 2022, our group demonstrated that DCNBT-IDT exhibited optimal thermodynamic miscibility with P3HT, resulting in a well-defined nanofiber phase-separated morphology. This system achieved a record PCE of 7.35% for P3HT-based all-PSCs, thereby setting a new benchmark for P3HT-based all-PSCs.[140] Inspired by this, Liang *et al.* reported a new polymer acceptor IDTBTC8-CN, utilizing IDT and monocyano-substituted benzothiadiazole (BT-CN) as building blocks. By incorporating a CN group into the polymer backbone, IDTBTC8-CN exhibited downshifted energy levels (E_{LUMO}/E_{HOMO} = −3.40 eV/−5.43 eV) compared to its non-cyano counterpart IDTBTC8 (E_{LUMO}/E_{HOMO} = −3.20 eV/−5.29 eV). Moreover, the enhanced miscibility in the P3HT:IDTBTC8-CN blend yielded an optimal bicontinuous interpenetrating network morphology. Consequently, a higher PCE of 8.30% was achieved in the P3HT:IDTBTC8-CN blend, in sharp contrast to that of the IDTBTC8-based system (1.21%).[141]

With the success of polymerized small-molecule acceptors (PSMAs) in all-PSCs,[142–145] researchers have explored the potential of PSMAs as replacements for traditional donor–acceptor (D–A) polymer acceptors in combination with P3HT. However, no effective optimization methods have been identified to match the popular PSMAs in P3HT-based all-PSCs, which is mainly ascribed to the mismatch of energy levels and difficulty in morphology optimization.[146] Consequently, researchers have developed novel P3HT derivatives that feature matched energy levels and appropriate thermodynamic miscibility with state-of-the-art PSMAs to obtain high-efficiency PT-based all-PSCs.

To finely tune the energy levels and crystallinity of polythiophene, making it more compatible with PSMA, An *et al.* reported a new polythiophene (PFTVT-T) for high-performance all-PSCs. The slightly twisted backbone of PFETVT-T effectively suppressed excessive molecular aggregation, thereby enhancing its miscibility with the polymer acceptor L15.[82] Consequently, the all-PSCs utilizing PFETVT-T:L15 achieved a J_{sc} of 19.74 mA cm^{-2}, an FF of 0.64, and an impressive PCE of 11.81%. Additionally, the PFETVT-T:L15-based devices demonstrated excellent photostability, maintaining 90% of their initial PCE after 500 hours of continuous illumination under white LED light (100 mW cm^{-2}).

Note that the intermolecular interaction between a donor and an acceptor can greatly affect the blending morphology and device efficiency of OSCs. Ma *et al.* systematically investigated the intermolecular interactions between PTs and polymer acceptor PY-IT, establishing a correlation between the chemical structure and blend compatibility. The introduction of ester groups in PDCBT reduced its energy levels (E_{LUMO}/E_{HOMO} = −2.84 eV/−5.35 eV) compared to the classical donor P3HT (E_{LUMO}/E_{HOMO} = −2.43 eV/−5.12 eV).[115] This modification also resulted in red-shifted absorption spectra from P3HT to PDCBT, accompanied by a distinct aggregation peak in the PDCBT film, indicating a more ordered intermolecular packing. As discussed in Section 3.1, the ester groups in PDCBT elevated its electrostatic potential (ESP), enhancing compatibility with PY-IT and reducing intermolecular interactions between the donor and acceptor (Fig. 12a). Consequently, the PDCBT:PY-IT blend film exhibited purer domains and optimal phase separation (Fig. 12b), which mitigated bimolecular recombination and improved the PCE of the device to 15.3%.

3.5 PT-based large-area OSCs

The development of low-cost OSCs requires careful consideration of two key factors: material selection and manufacturing methods. Polythiophene donor materials offer a cost-effective solution, while gravure printing provides a large-area fabrication technique with high-speed, high-precision, low-cost advantages, and two-dimensional patterning capability.

In 2023, Wang *et al.* reported large-area OSC modules with a device area of 22.1 cm^2, fabricated by the blade coating techniques based on the high-performance PT derivative PTVT-

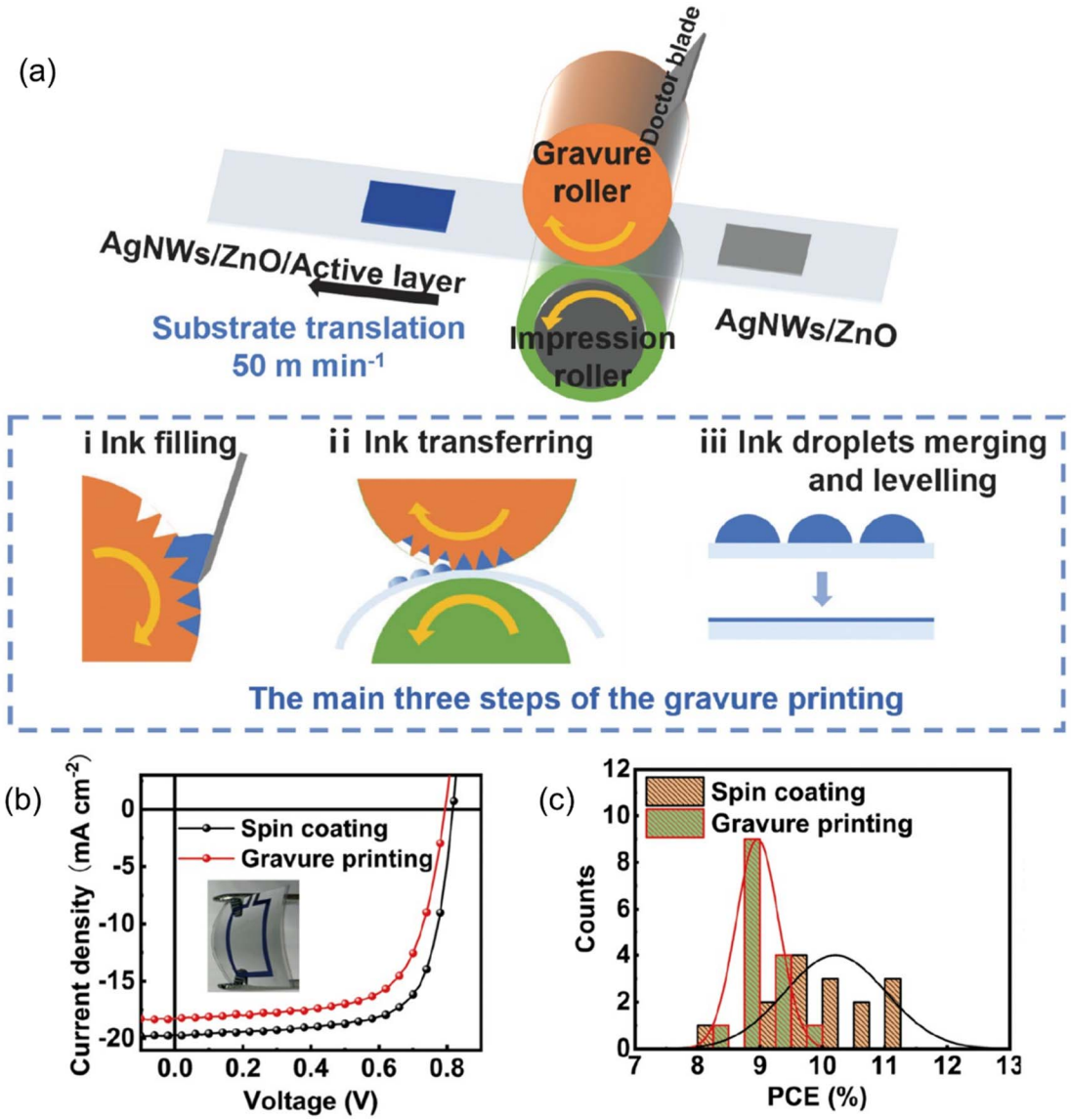

Fig. 13 (a) Schematic diagram of the fabrication of active layer films by gravure printing and the three main steps in the gravure process: (i) the doctor blade forces the ink to fill the gravure cavities; (ii) the ink is transferred from the cavities of the gravure roller to the substrate; (iii) ink droplets level on the substrate. (b) *J*–*V* curves and (c) efficiency statistical distributions of P5TCN-F25-based OSCs fabricated by spin-coated and gravure-printed active layers.[147]

T. The module consisted of six sub-cells, each with an area of 3.5 cm^2, connected in series. By optimizing the patterning conditions, the module achieved a dead area width of 0.45 mm and a geometric fill factor (GFF) of 94%. The manufactured 22.1 cm^2 OSC modules delivered PCEs of 11.2%, 11.8%, 12.1%, 23.1%, and 20.3% under AM 1.5 G illumination, natural light during cloudy weather, natural light in shadow, laser irradiation, and indoor light, respectively.[79]

To develop low-cost and large-area PT-based OSCs, Qi *et al.* reported flexible P5TCN-F25-based OSCs *via* roll-to-roll (R2R) gravure printing (Fig. 13a). The viscosity of the active layer ink was regulated by adjusting the concentration of the ink, which significantly reduced flow stripe formation and resulted in a uniform film. To improve the PCE of gravure-printed devices, they further investigated the influence of ink temperature on the film morphology. Atomic force microscopy (AFM) phase images indicated that the excessive aggregation of gravure-printed active layer film morphology was inhibited with the increasing temperature of the ink. Consequently, 1 cm^2 flexible OSCs fabricated *via* R2R gravure printing demonstrated a PCE of 10.55%, which is comparable to that of spin-coated devices (Fig. 13b and c). This study highlighted the suitability of low-cost polythiophenes for R2R gravure printing, suggesting their potential application in future low-cost OSCs.[147]

3.6 Stability of PT-based OSCs

Solar cells featuring polythiophenes as donors are one of the optoelectronic devices that hold notable promise for

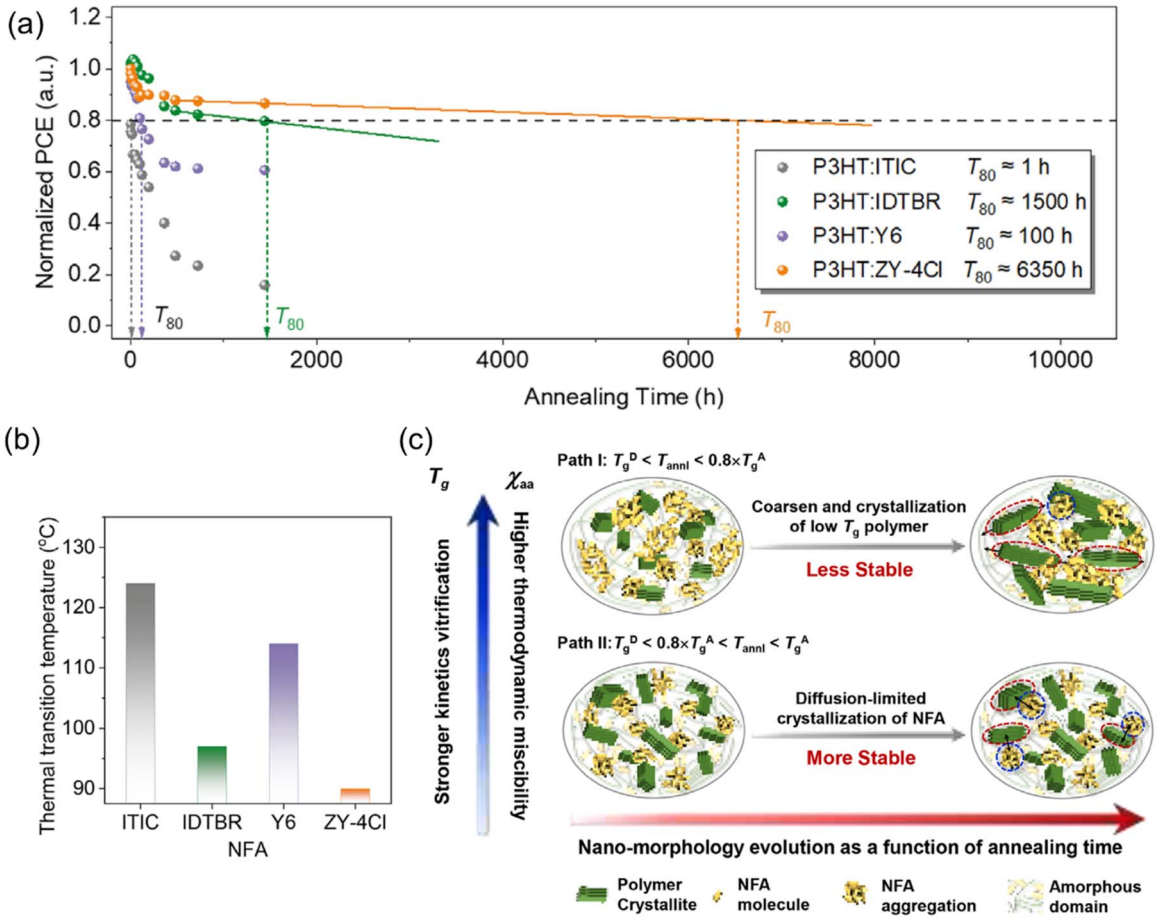

Fig. 14 (a) Normalized power conversion efficiencies (PCEs) of the four P3HT:NFA devices *versus* the annealing time of the active layer under continuous thermal heating at 80 °C. (b) The plot of the thermal transition temperatures (T_g) of the four nonfullerene acceptors. (c) Schematic illustrations of two paths of nanomorphology evolution as a function of time. In this work, P3HT:ITIC (T_g^D (T_g of the crystalline polymer donor) < $T_{annl} < 0.8 \times T_g^A$ (T_g of the small molecule acceptor)) and P3HT:ZY-4Cl ($T_g^D < 0.8 \times T_g^A < T_{annl} < T_g^A$) belong to the typical cases of paths I and II, respectively.[112]

commercial application, benefiting from the minimal synthetic complexity and excellent scalability. Compared with widely studied fused-ring polymer donors, polythiophenes offer distinct advantages in terms of device stability, attributed to their unique phase behaviors. Therefore, establishing new material guidelines that balance high device performance with long-term stability is crucial for advancing these emerging polythiophene OSCs.[148,149]

The miscibility between a donor and an acceptor significantly impacts the stability of film morphology and device performance. In 2020, Liang *et al.* established a comprehensive relationship between the molecular structure, miscibility, and device stability in OSCs based on PBDCT-Cl. Specifically, OSCs incorporating PDCBT-Cl:IDIC, PDCBT-Cl:ITIC-Th1, and PDCBT-Cl:IT4F exhibited poor stability, with approximately 20% performance degradation after 100 hours of aging under inert conditions. This instability was attributed to the significant deviation of the film morphology from thermodynamic equilibrium. Conversely, the OSC based on PDCBT-Cl:ITIC exhibited superior stability with less than 10% degradation, due to its morphology being closer to equilibrium. Notably, the highly miscible PDCBT-Cl:Y6 blend maintained its photovoltaic performance after 100 hours of aging. This research highlights the importance of optimizing donor–acceptor miscibility to enhance device stability.[114]

Furthermore, the same group reported that the aggregated rigidity in blend solutions is also associated with the stability of solid films and device performance. The authors proposed that higher molecular ordered polymer systems can yield more rigid aggregates in the blend solution, which subsequently promotes higher crystallinity and improved thermal stability in blend films. Compared to fused-ring polymers such as PM6, the polythiophene P5TCN exhibited rigid aggregates in solution, thus leading to stable crystalline domains and high stability OSCs (with a total PCE decay of ~36% during a long-term aging period of ~2300 hours).[123]

Beyond molecular interactions, the glass transition temperature (T_g) represents a critical thermal property of organic photovoltaic materials, playing a pivotal role in predicting morphological stability, which corresponds to the onset of

backbone relaxation processes. Gao *et al.* investigated the interplay between thermodynamic properties, kinetic factors, morphological characteristics, and thermal stability in P3HT-based OSCs. During continuous thermal annealing at 80 °C, the T_{80} values for P3HT:ITIC, P3HT:IDTBR, P3HT:Y6, and P3HT:ZY-4Cl-based OSCs were 1, 1500, 100, and 6350 hours, respectively, highlighting significant differences in thermal stability among the systems (Fig. 14a). For the most stable P3HT:ZY-4Cl blend, the PCE decreased by approximately 14% after over 1500 hours of thermal annealing. The excellent morphological stability of the P3HT:ZY-4Cl blends was attributed to the diffusion-limited crystallization process of ZY-4Cl, which fostered a kinetic equilibrium state of mutual restriction. Specifically, the local diffusion of ZY-4Cl occurred since the annealing temperature (80 °C) was above $0.8 \times T_g$ (~72 °C) but below T_g (~90 °C), leading to a fine-grained nanostructure that remained stable over time (Fig. 14c, path II). In contrast, the P3HT:ITIC system held hindered P3HT crystallization and inefficient charge transport due to the stronger vitrification effect and relatively good miscibility (Fig. 14c, path I). This realization of high thermal stability and efficiency demonstrates the remarkable potentials of simple PT:NFA pairs for electronic applications.[112]

4. Summary and outlook

Polythiophene-based OSCs have achieved significant progress in recent years. However, attaining both high efficiency and environmental sustainability remains a critical challenge. This paper highlights four key research priorities: (1) establishing fundamental studies of PTs and their blend films, (2) the development of eco-friendly processing methods, (3) the exploration of cost-effective NFAs, and (4) the enhancement of device stability.

4.1 Establishing fundamental understanding of PTs and their blends

For PT-based OSCs, the current PCE still lags behind that of state-of-the-art donors, which is largely due to the difficulty in morphology optimization. The non-fused conjugated backbones of PTs could induce torsional defects along their main chains, leading to weak preaggregation in solution and hypermiscibility with NFAs in the solid-state blend film. To further improve the efficiency of PT-based OSCs, comprehensive investigations into the fundamental physical properties of PTs and their blend systems are imperative. Specifically, systematic computational modeling (*e.g.*, time-dependent density functional theory and molecular dynamics simulations) enables precise prediction of optoelectronic properties and elucidates morphology-formation dynamics, which will provide crucial insights for active layer optimization. Advanced characterization methodologies, such as *in situ* morphological monitoring and neutron scattering techniques, will offer powerful tools to elucidate the structure–property relationships between the molecular structure and film morphology, thereby guiding the design of more efficient PT systems.

4.2 Development of eco-friendly processible PT:NFA systems

Another critical research direction should focus on environmentally sustainable PT-based OSCs. The utilization of green solvents in the fabrication process could significantly reduce the ecological impact of production. Notably, recent studies have demonstrated that machine learning (ML) and big data models can predict material solubility. By integrating solubility parameters with drying kinetics, which elucidates the solvent removal process, researchers can develop comprehensive models that simultaneously address dissolution dynamics and drying mechanisms. This strategy offers a robust framework for achieving high-performance, large-area PT-based OSCs.

4.3 Development of low-cost NFAs to match PTs

The continuous exploration and development of structurally simplified NFAs present an opportunity to reduce manufacturing costs without compromising device performance. Recent advances in non-fused NFAs, which are synthesized from commercially available materials, demonstrate significant cost advantages. These acceptors can be engineered to match the energy levels of PTs, thereby improving charge transfer efficiency and device performance. Additionally, adopting sustainable synthesis routes and utilizing abundant raw materials for materials production can contribute to cost reduction while promoting environmental sustainability.

4.4 Enhancing long-term stability of PT-based OSCs

Long-term stability of OSCs is paramount for their commercial viability. Research efforts should focus on investigating the degradation mechanisms of both PT donors and NFAs under operational conditions. Strategies such as interlayer/electrode engineering, encapsulation techniques, and the development of intrinsically stable materials could mitigate degradation and prolong device lifetimes.

Data availability

No primary research results, software or code have been included and no new data were generated or analysed as part of this review.

Author contributions

All of the authors contributed to the manuscript preparation. X. Y. and C. D. conceived the outline of the manuscript. X. Y., J. L., W. D., and X. Z. wrote the original draft of the manuscript. X. Y., J. L., and C. D. discussed and helped revise the manuscript.

Conflicts of interest

There are no conflicts to declare.

Acknowledgements

This research was financially supported by the Guangdong Basic and Applied Basic Research Foundation (2022B1515120008), the National Natural Science Foundation of China (22275058 and 52403225), the Guangdong Innovative and Entrepreneurial Research Team Program (2019ZT08L075), the China Postdoctoral Science Foundation (2023TQ0120, GZB20230223, and 2024M750945), the Fundamental Research Funds for the Central Universities (2024ZYGXZR063), the Ningbo Natural Science Foundation (2024J111) and the Scientific Research Fund of Zhejiang Provincial Education Department (Y202456587).

References

1 J. Yi, G. Zhang, H. Yu and H. Yan, *Nat. Rev. Mater.*, 2023, **9**, 46–62.
2 H. Yu, J. Wang, Q. Zhou, J. Qin, Y. Wang, X. Lu and P. Cheng, *Chem. Soc. Rev.*, 2023, **52**, 4132–4148.
3 P. Ding, D. Yang, S. Yang and Z. Ge, *Chem. Soc. Rev.*, 2024, **53**, 2350–2387.
4 P. Cheng, G. Li, X. Zhan and Y. Yang, *Nat. Photonics*, 2018, **12**, 131–142.
5 J. Hou, O. Inganas, R. H. Friend and F. Gao, *Nat. Mater.*, 2018, **17**, 119–128.
6 G. Zhang, F. R. Lin, F. Qi, T. Heumuller, A. Distler, H. J. Egelhaaf, N. Li, P. C. Y. Chow, C. J. Brabec, A. K. Jen and H. L. Yip, *Chem. Rev.*, 2022, **122**, 14180.
7 H. Yao and J. Hou, *Angew. Chem., Int. Ed.*, 2022, **61**, 202209021.
8 W. Wei, X. Zhou, M. Yang, B. Wu and C. Duan, *Sci. China Mater.*, 2024, **68**, 1–20.
9 P. Jiang, Y. Liu, J. Song and Z. Bo, *Acc. Chem. Res.*, 2024, **57**, 3419–3432.
10 Z. Luo, T. Xu, C. e. Zhang and C. Yang, *Energy Environ. Sci.*, 2023, **16**, 2732–2758.
11 Y. Jiang, S. Sun, R. Xu, F. Liu, X. Miao, G. Ran, K. Liu, Y. Yi, W. Zhang and X. Zhu, *Nat. Energy*, 2024, **9**, 975–986.
12 L. Zhu, M. Zhang, G. Zhou, Z. Wang, W. Zhong, J. Zhuang, Z. Zhou, X. Gao, L. Kan, B. Hao, F. Han, R. Zeng, X. Xue, S. Xu, H. Jing, B. Xiao, H. Zhu, Y. Zhang and F. Liu, *Joule*, 2024, **8**, 3153–3168.
13 C. Chen, L. Wang, W. Xia, K. Qiu, C. Guo, Z. Gan, J. Zhou, Y. Sun, D. Liu, W. Li and T. Wang, *Nat. Commun.*, 2024, **15**, 6865.
14 R. Po, G. Bianchi, C. Carbonera and A. Pellegrino, *Macromolecules*, 2015, **48**, 453–461.
15 M. Moser, A. Wadsworth, N. Gasparini and I. McCulloch, *Adv. Energy Mater.*, 2021, **11**, 2100056.
16 R. Po, A. Bernardi, A. Calabrese, C. Carbonera, G. Corso and A. Pellegrino, *Energy Environ. Sci.*, 2014, **7**, 925–943.
17 M. Zhang, X. Guo, W. Ma, H. Ade and J. Hou, *Adv. Mater.*, 2015, **27**, 4655–4660.
18 Q. Liu, Y. Jiang, K. Jin, J. Qin, J. Xu, W. Li, J. Xiong, J. Liu, Z. Xiao, K. Sun, S. Yang, X. Zhang and L. Ding, *Sci. Bull.*, 2020, **65**, 272–275.
19 C. Duan and L. Ding, *Sci. Bull.*, 2020, **65**, 1422–1424.
20 C. Cui and Y. Li, *Energy Environ. Sci.*, 2019, **12**, 3225–3246.
21 L. Zhang, X. Huang, C. Duan, Z. Peng, L. Ye, N. Kirby, F. Huang and Y. Cao, *J. Mater. Chem. A*, 2021, **9**, 556.
22 D. Yuan, F. Pan, L. Zhang, H. Jiang, M. Chen, W. Tang, G. Qin, Y. Cao and J. Chen, *Sol. RRL*, 2020, **4**, 2000062.
23 B. Yin, Z. Chen, S. Pang, X. Yuan, Z. Liu, C. Duan, F. Huang and Y. Cao, *Adv. Energy Mater.*, 2022, **12**, 2104050.
24 Q. Jiang, X. Yuan, Y. Li, Y. Luo, J. Zhu, F. Zhao, Y. Zhang, W. Wei, H. Feng, H. Li, J. Wu, Z. Ma, Z. Tang, F. Huang, Y. Cao and C. Duan, *Angew. Chem., Int. Ed.*, 2025, **64**, 202416883.
25 X. Zhang, X. Wu, J. Zhang, X. Kong, J. Li, A. Li, Z. Li, X. Li, M. Zhang, G. Yang, Y. Li and C. Sun, *ACS Nano*, 2025, **19**, 900–910.
26 J. Ren, P. Bi, J. Zhang, J. Liu, J. Wang, Y. Xu, Z. Wei, S. Zhang and J. Hou, *Natl. Sci. Rev.*, 2021, **8**, nwab031.
27 T. P. Osedach, T. L. Andrew and V. Bulović, *Energy Environ. Sci.*, 2013, **6**, 711–718.
28 M. T. Dang, L. Hirsch and G. Wantz, *Adv. Mater.*, 2011, **23**, 3597–3602.
29 Q. Wang, Y. Qin, M. Li, L. Ye and Y. Geng, *Adv. Energy Mater.*, 2020, **10**, 2002572.
30 U. Mehmood, A. Al-Ahmed and I. A. Hussein, *Renewable Sustainable Energy Rev.*, 2016, **57**, 550–561.
31 M. Zhang, X. Guo, W. Ma, H. Ade and J. Hou, *Adv. Mater.*, 2014, **26**, 5880–5885.
32 H. Yao, D. Qian, H. Zhang, Y. Qin, B. Xu, Y. Cui, R. Yu, F. Gao and J. Hou, *Chin. J. Chem.*, 2018, **36**, 491–494.
33 K. Xian, Y. Geng and L. Ye, *Joule*, 2022, **6**, 941–944.
34 L. Ye, H. Ke and Y. Liu, *Trends Chem.*, 2021, **3**, 1074–1087.
35 X. Yuan, Y. Zhao, D. Xie, L. Pan, X. Liu, C. Duan, F. Huang and Y. Cao, *Joule*, 2022, **6**, 647–661.
36 Q. Ai, Z. Lin, X. Wu, Y. Zhu, K. Wang, X. Li, J. Zhang, D. He, Y. Li and F. Zhao, *J. Mater. Chem. A*, 2024, **12**, 10984–10990.
37 E. E. Sheina, J. Liu, M. C. Iovu, D. W. Laird and R. D. McCullough, *Macromolecules*, 2004, **37**, 3526.
38 R. Miyakoshi, A. Yokoyama and T. Yokozawa, *J. Am. Chem. Soc.*, 2005, **127**, 17542–17547.
39 Y. Qiu, J. C. Worch, A. Fortney, C. Gayathri, R. R. Gil and K. J. T. Noonan, *Macromolecules*, 2016, **49**, 4757–4762.
40 M. Rangel, M. Güizado-Rodríguez, J. L. Maldonado, R. Olayo-Valles, V. Barba and J. U. Reveles, *Polymer*, 2020, **193**, 122348.
41 Y. Liu, K. Xian, Z. Peng, M. Gao, Y. Shi, Y. Deng, Y. Geng and L. Ye, *J. Mater. Chem. A*, 2021, **9**, 19874–19885.
42 Y. Liu, K. Xian, R. Gui, K. Zhou, J. Liu, M. Gao, W. Zhao, X. Jiao, Y. Deng, H. Yin, Y. Geng and L. Ye, *Macromolecules*, 2021, **55**, 133–145.
43 K. Okamoto and C. K. Luscombe, *Polym. Chem.*, 2011, **2**, 2424.
44 K. A. Mazzio, A. H. Rice, M. M. Durban and C. K. Luscombe, *J. Phys. Chem. C*, 2015, **119**, 14911.
45 Y. Liu, K. Xian, X. Zhang, M. Gao, Y. Shi, K. Zhou, Y. Deng, J. Hou, Y. Geng and L. Ye, *Macromolecules*, 2022, **55**, 3078–3086.

46 X. Zhang, T. Zhang, Z. Liang, Y. Shi, S. Li, C. Xu, M. Li, L. Ye, J. Hou and Y. Geng, *Adv. Energy Mater.*, 2024, **14**, 2402239.
47 Z. Liang, A. Neshchadin, Z. Zhang, F.-G. Zhao, X. Liu and L. Yu, *Polym. Chem.*, 2023, **14**, 4611–4625.
48 H. Bohra and M. Wang, *J. Mater. Chem. A*, 2017, **5**, 11550–11571.
49 B.-w. Ma, Q.-q. Shi and H. Huang, *Acta Polym. Sin.*, 2023, **54**, 791–802.
50 L.-J. Yang, N. Chen, X.-M. Huang, Y. Wu, H. Liu, P. Liu, L. Hu, Z.-F. Li and S.-Y. Liu, *ACS Appl. Polym. Mater.*, 2023, **5**, 7340–7349.
51 X. Zhang, Y. Shi, Y. Deng and Y. Geng, *Chin. J. Chem.*, 2023, **41**, 2908–2924.
52 T. Menda, T. Mori and T. Yasuda, *Polym. J.*, 2020, **53**, 403–408.
53 X. e. Jia, Z. Chen, C. Duan, Z. Wang, Q. Yin, F. Huang and Y. Cao, *J. Mater. Chem. C*, 2019, **7**, 314.
54 J. Xiao, X. Jia, C. Duan, F. Huang, H. L. Yip and Y. Cao, *Adv. Mater.*, 2021, **33**, 2008158.
55 X. e. Jia, G. Liu, S. Chen, Z. Li, Z. Wang, Q. Yin, H.-L. Yip, C. Yang, C. Duan, F. Huang and Y. Cao, *ACS Appl. Energy Mater.*, 2019, **2**, 7572.
56 Q. Xu, C. Chang, W. Li, B. Guo, X. Guo and M. Zhang, *Acta Phys.-Chim. Sin.*, 2019, **35**, 268–274.
57 C. Yang, S. Zhang, J. Ren, P. Bi, X. Yuan and J. Hou, *Chin. Chem. Lett.*, 2021, **32**, 2274–2278.
58 D. Jeong, G. U. Kim, D. Lee, S. Seo, S. Lee, D. Han, H. Park, B. Ma, S. Cho and B. J. Kim, *Adv. Energy Mater.*, 2022, **12**, 2201603.
59 Y. Qin, M. A. Uddin, Y. Chen, B. Jang, K. Zhao, Z. Zheng, R. Yu, T. J. Shin, H. Y. Woo and J. Hou, *Adv. Mater.*, 2016, **28**, 9416–9422.
60 H. Zhang, S. Li, B. Xu, H. Yao, B. Yang and J. Hou, *J. Mater. Chem. A*, 2016, **4**, 18043–18049.
61 L.-Y. Su, Y.-L. Zhou, Y.-T. Chen, G.-L. Chen, K.-W. Tseng, N. Tukachev, A. Zhugayevych, S. Tretiak and L. Wang, *Polymer*, 2025, **326**, 128336.
62 Q. Wang, M. Li, X. Zhang, Y. Qin, J. Wang, J. Zhang, J. Hou, R. A. J. Janssen and Y. Geng, *Macromolecules*, 2019, **52**, 4464–4474.
63 Q. Wang, M. Li, Z. Peng, N. Kirby, Y. Deng, L. Ye and Y. Geng, *Sci. China: Chem.*, 2021, **64**, 478–487.
64 M. Cao, R. An, Z. Peng, Q. Zhang, H. Li, X. Wu, H. Tong and L. Wang, *Polym. Chem.*, 2025, **16**, 2298–2308.
65 X. Zhou, Z. Zhang, A. D. Hendsbee, J. H. L. Ngai, P. Kumar, S. Ye, D. S. Seferos and Y. Li, *RSC Adv.*, 2019, **9**, 30496–30502.
66 K. He, P. Kumar, M. Abd-Ellah, H. Liu, X. Li, Z. Zhang, J. Wang and Y. Li, *Macromolecules*, 2020, **53**, 8796–8808.
67 B. Zhang, Y. Yu, J. Zhou, Z. Wang, H. Tang, S. Xie, Z. Xie, L. Hu, H. L. Yip, L. Ye, H. Ade, Z. Liu, Z. He, C. Duan, F. Huang and Y. Cao, *Adv. Energy Mater.*, 2020, **10**, 1904247.
68 X. Yuan, Y. Zhao, T. Zhan, J. Oh, J. Zhou, J. Li, X. Wang, Z. Wang, S. Pang, P. Cai, C. Yang, Z. He, Z. Xie, C. Duan, F. Huang and Y. Cao, *Energy Environ. Sci.*, 2021, **14**, 5530–5540.
69 Y. Zhang, L. Pan, Z. Peng, W. Deng, B. Zhang, X. Yuan, Z. Chen, L. Ye, H. Wu, X. Gao, Z. Liu, C. Duan, F. Huang and Y. Cao, *J. Mater. Chem. A*, 2021, **9**, 13522–13530.
70 X. Yuan, B. Zhang, Y. Li, F. Zhao, W. Wei, Y. Zhang, J. Li, Y. Tian, Z. Ma, Z. Tang, Z. Liu, F. Huang, Y. Cao and C. Duan, *ACS Appl. Mater. Interfaces*, 2025, **17**, 6659–6667.
71 X. Yuan, Y. Zhao, Y. Zhang, D. Xie, W. Deng, J. Li, H. Wu, C. Duan, F. Huang and Y. Cao, *Adv. Funct. Mater.*, 2022, **32**, 2201142.
72 J. Li, D. Xie, X. Yuan, Y. Li, W. Wei, Y. Zhang, H. Feng, X. Luo, J. Zhu, Z. Qin, J. Zhong, l. zhang, H. Li, W. Zhang, Y. Zhang, F. Huang, Y. Cao and C. Duan, *Energy Environ. Sci.*, 2025, **18**, 4384–4395.
73 P. Prins, L. P. Candeias, A. J. J. M. van Breemen, J. Sweelssen, P. T. Herwig, H. F. M. Schoo and L. D. A. Siebbeles, *Adv. Mater.*, 2005, **17**, 718–723.
74 I. W. Hwang, Q. H. Xu, C. Soci, B. Chen, A. K. Y. Jen, D. Moses and A. J. Heeger, *Adv. Funct. Mater.*, 2007, **17**, 563–568.
75 X. Zhou, Z. Zhang, A. D. Hendsbee, J. H. L. Ngai, P. Kumar, S. Ye, D. S. Seferos and Y. Li, *RSC Adv.*, 2019, **9**, 30496–30502.
76 L. Huo, T. L. Chen, Y. Zhou, J. Hou, H.-Y. Chen, Y. Yang and Y. Li, *Macromolecules*, 2009, **42**, 4377–4380.
77 B. Lim, K. J. Baeg, H. G. Jeong, J. Jo, H. Kim, J. W. Park, Y. Y. Noh, D. Vak, J. H. Park, J. W. Park and D. Y. Kim, *Adv. Mater.*, 2009, **21**, 2808–2814.
78 P. Bi, J. Ren, S. Zhang, J. Wang and J. Hou, *Polymer*, 2020, **209**, 122900.
79 J. Wang, Y. Wang, J. Li, Y. Yu, P. Bi, J. Qiao, Z. Chen, C. Wang, W. Wang, J. Dai, X. Hao, S. Zhang and J. Hou, *Angew. Chem., Int. Ed.*, 2023, **62**, 202314362.
80 B. Liu, S. Gámez-Valenzuela, J.-W. Lee, B. Li, W. Yang, K. Wang, Z. Zhong, J. Yang, Z. Wang, C. Xu, H. Sun, B. J. Kim and X. Guo, *ACS Energy Lett.*, 2024, **9**, 3727–3736.
81 P. Bi, J. Ren, S. Zhang, J. Wang, Z. Chen, M. Gao, Y. Cui, T. Zhang, J. Qin, Z. Zheng, L. Ye, X. Hao and J. Hou, *Nano Energy*, 2022, **100**, 107463.
82 M. An, Q. Bai, S. Y. Jeong, J. Ding, C. Zhao, B. Liu, Q. Liang, Y. Wang, G. Zhang, H. Y. Woo, X. Qiu, L. Niu, X. Guo and H. Sun, *Adv. Energy Mater.*, 2023, **13**, 2301110.
83 T. N. Phan, J. W. Lee, T. H. Nguyen, H. Jeon and B. J. Kim, *ACS Appl. Mater. Interfaces*, 2024, **16**, 63861–63870.
84 H. Li, J. Ren, L. Ma, Z. Chen, Y. Yu, J. Wang and S. Zhang, *Chin. J. Chem.*, 2024, **42**, 3405–3413.
85 J. W. Lee, T. N. L. Phan, E. S. Oh, H. G. Lee, T. S. Kim and B. J. Kim, *Adv. Funct. Mater.*, 2023, **33**, 2305851.
86 Y. Gao, M. Cui, S. Qu, H. Zhao, Z. Shen, F. Tan, Y. Dong, C. Qin, Z. Wang, W. Zhang, Z. Wang and Y. Lei, *Small*, 2022, **18**, 2104623.
87 B. Wang, Y. Kong, X. K. Ye, S. Ye, T. Chen, S. Wang, S. Li, M. Shi, J. T. Xu and H. Chen, *ACS Appl. Mater. Interfaces*, 2025, **17**, 7707–7715.
88 L. Ma, S. Zhang, J. Ren, G. Wang, J. Li, Z. Chen, H. Yao and J. Hou, *Angew. Chem., Int. Ed.*, 2023, **62**, 202214088.
89 O. Gidron, A. Dadvand, Y. Sheynin, M. Bendikov and D. F. Perepichka, *Chem. Commun.*, 2011, **47**, 1976–1978.

90 P. Huang, J. Du, M. C. Biewer and M. C. Stefan, *J. Mater. Chem. A*, 2015, **3**, 6244.
91 X. Li, X. Duan, Z. Liang, L. Yan, Y. Yang, J. Qiao, X. Hao, C. Zhang, J. Zhang, Y. Li, F. Huang and Y. Sun, *Adv. Energy Mater.*, 2022, **12**, 2103684.
92 X. Li, Y. Li, Y. Zhang and Y. Sun, *Small Sci.*, 2022, **2**, 2200006.
93 X. Yuan, H. Chen, S. Kim, Y. Chen, Y. Zhang, M. Yang, Z. Chen, C. Yang, H. Wu, X. Gao, Z. Liu and C. Duan, *Adv. Energy Mater.*, 2023, **13**, 2204394.
94 D. Zhu, X. Bao, Q. Zhu, C. Gu, M. Qiu, S. Wen, J. Wang, B. Shahida and R. Yang, *Energy Environ. Sci.*, 2017, **10**, 614–620.
95 X. Yuan, Q. Wang, D. Zhu, B. Shahid and R. Yang, *Macromol. Rapid Commun.*, 2019, **40**, 1900035.
96 D. Zhu, X. Bao, D. Ouyang, J. Wang, X. Yuan, Q. Wang, D. Zhou, S. Wen and R. Yang, *Nano Energy*, 2017, **40**, 495–503.
97 Y. Huang, E. J. Kramer, A. J. Heeger and G. C. Bazan, *Chem. Rev.*, 2014, **114**, 7006–7043.
98 H. Lee, C. Park, D. H. Sin, J. H. Park and K. Cho, *Adv. Mater.*, 2018, **30**, 1800453.
99 F. Zhao, C. Wang and X. Zhan, *Adv. Energy Mater.*, 2018, **8**, 1703147.
100 L. Ye, B. A. Collins, X. Jiao, J. Zhao, H. Yan and H. Ade, *Adv. Energy Mater.*, 2018, **8**, 1703058.
101 L. Ye, H. Hu, M. Ghasemi, T. Wang, B. A. Collins, J. H. Kim, K. Jiang, J. H. Carpenter, H. Li, Z. Li, T. McAfee, J. Zhao, X. Chen, J. L. Y. Lai, T. Ma, J. L. Bredas, H. Yan and H. Ade, *Nat. Mater.*, 2018, **17**, 253–260.
102 Z. Li, H. Yao, L. Ma, J. Wang, Z. Bi, S. Wang, S. Seibt, T. Zhang, Y. Xu, J. Ren, Y. Xiao, C. An, W. Ma and J. Hou, *Adv. Funct. Mater.*, 2023, **33**, 2300202.
103 J. He, Z. Liang, L. Lin, S. Liang, J. Xu, W. Ni, M. Li and Y. Geng, *Polymer*, 2023, **274**, 125890.
104 B. Zhang, Y. Yu, Z. Liu, X. Liu, C. Duan and F. Huang, *Acta Polym. Sin.*, 2020, **51**, 620–631.
105 Q. Wang, Z. Hu, Z. Wu, Y. Lin, L. Zhang, L. Liu, Y. Ma, Y. Cao and J. Chen, *ACS Appl. Mater. Interfaces*, 2020, **12**, 4659–4672.
106 D. Yuan, A. Zhong, L. Zhang, W. Chen, H. Jiang, Q. Ye, C. Liu, J. Chen and Y. Cao, *Synth. Met.*, 2019, **256**, 116116.
107 X. Xue, K. Weng, F. Qi, Y. Zhang, Z. Wang, J. Ali, D. Wei, Y. Sun, F. Liu, M. Wan, J. Liu and L. Huo, *Adv. Energy Mater.*, 2019, **9**, 1802686.
108 J. Liang, M. Pan, G. Chai, Z. Peng, J. Zhang, S. Luo, Q. Han, Y. Chen, A. Shang, F. Bai, Y. Xu, H. Yu, J. Y. L. Lai, Q. Chen, M. Zhang, H. Ade and H. Yan, *Adv. Mater.*, 2020, **32**, 2003500.
109 W. Li, L. Yang, J. R. Tumbleston, L. Yan, H. Ade and W. You, *Adv. Mater.*, 2014, **26**, 4456–4462.
110 Y. Li, X. Yuan, S. Kim, Y. Zhang, D. Xie, X. Tan, C. Yang, X. Huang, F. Huang, Y. Cao and C. Duan, *ACS Appl. Mater. Interfaces*, 2023, **15**, 29341.
111 C. Yang, S. Zhang, J. Ren, M. Gao, P. Bi, L. Ye and J. Hou, *Energy Environ. Sci.*, 2020, **13**, 2864–2869.
112 M. Gao, Y. Liu, K. Xian, Z. Peng, K. Zhou, J. Liu, S. Li, F. Xie, W. Zhao, J. Zhang, X. Jiao and L. Ye, *Aggregate*, 2022, **3**, e190.
113 Y. Li, Y. Zhang, B. Wu, S. Pang, X. Yuan, C. Duan, F. Huang and Y. Cao, *Sol. RRL*, 2022, **6**, 2200073.
114 Z. Liang, M. Li, Q. Wang, Y. Qin, S. J. Stuard, Z. Peng, Y. Deng, H. Ade, L. Ye and Y. Geng, *Joule*, 2020, **4**, 1278–1295.
115 L. Ma, H. Yao, J. Zhang, Z. Chen, J. Wang, J. Qiao, S. Wang, Z. Bi, Z. Li, X. Hao, Z. Wei, W. Ma and J. Hou, *Chem*, 2023, **9**, 2518–2529.
116 C. McDowell, M. Abdelsamie, M. F. Toney and G. C. Bazan, *Adv. Mater.*, 2018, **30**, 1707114.
117 D. Hu, H. Tang, C. Chen, D. J. Lee, S. Lu, G. Li, H. Y. Hsu and F. Laquai, *Adv. Mater.*, 2024, **36**, 2406949.
118 C. Yang, R. Yu, C. Liu, H. Li, S. Zhang and J. Hou, *ChemSusChem*, 2021, **14**, 3607–3613.
119 K. An, W. Zhong and L. Ying, *Org. Electron.*, 2020, **82**, 105701.
120 M. Gao, J. Wu, X. Yuan, C. He, H. Jiang, W. Zhao, C. Duan, Y. Chen, Y. Ke, H. Yao and L. Ye, *Energy Environ. Sci.*, 2023, **16**, 5822–5831.
121 M. Gao, C. Sun, Y. Li, N. Li, H. Jiang, C. He, Y. Chen, W. Zhao, J. Hou and L. Ye, *Adv. Mater.*, 2024, **36**, 2406653.
122 X. Tan, Y. Li, X. Yuan, S. Kim, Y. Zhang, C. Yang, F. Huang, Y. Cao and C. Duan, *Sci. China: Chem.*, 2023, **66**, 2347.
123 M. Gao, J. Wu, X. Yuan, C. He, H. Jiang, W. Zhao, C. Duan, Y. Chen, Y. Ke, H. Yao and L. Ye, *Energy Environ. Sci.*, 2023, **16**, 5822–5831.
124 Z. Bi, C. Liu and W. Ma, *Adv. Funct. Mater.*, 2024, **34**, 2409315.
125 Q. Liang, X. Jiao, Y. Yan, Z. Xie, G. Lu, J. Liu and Y. Han, *Adv. Funct. Mater.*, 2019, **29**, 1807591.
126 J. Liu, S. Zeng, P. Jing, K. Zhao and Q. Liang, *J. Energy Chem.*, 2020, **51**, 333–341.
127 K. Zhou, Y. Wu, Y. Liu, X. Zhou, L. Zhang and W. Ma, *ACS Energy Lett.*, 2019, **4**, 1057–1064.
128 E. Zhou, J. Cong, Q. Wei, K. Tajima, C. Yang and K. Hashimoto, *Angew. Chem., Int. Ed.*, 2011, **50**, 2799–2803.
129 C. R. McNeill, J. J. M. Halls, R. Wilson, G. L. Whiting, S. Berkebile, M. G. Ramsey, R. H. Friend and N. C. Greenham, *Adv. Funct. Mater.*, 2008, **18**, 2309–2321.
130 Y. Zhou, Q. Yan, Y.-Q. Zheng, J.-Y. Wang, D. Zhao and J. Pei, *J. Mater. Chem. A*, 2013, **1**, 6609.
131 Q. Yang, H. Song, B. Gao, Y. Wang, Y. Fu, J. Yang, Z. Xie and L. Wang, *RSC Adv.*, 2014, **4**, 12579.
132 H. Sun, L. Wang, Y. Wang and X. Guo, *Chem.–Eur. J.*, 2019, **25**, 87–105.
133 X. Guo, A. Facchetti and T. J. Marks, *Chem. Rev.*, 2014, **114**, 8943–9021.
134 L. Gao, Z. G. Zhang, L. Xue, J. Min, J. Zhang, Z. Wei and Y. Li, *Adv. Mater.*, 2016, **28**, 1884.
135 L. Zhu, W. Zhong, C. Qiu, B. Lyu, Z. Zhou, M. Zhang, J. Song, J. Xu, J. Wang, J. Ali, W. Feng, Z. Shi, X. Gu, L. Ying, Y. Zhang and F. Liu, *Adv. Mater.*, 2019, **31**, 1902899.

136 J. R. Moore, S. Albert-Seifried, A. Rao, S. Massip, B. Watts, D. J. Morgan, R. H. Friend, C. R. McNeill and H. Sirringhaus, *Adv. Energy Mater.*, 2011, **1**, 230–240.
137 H. D. Kim, Y. Horiuchi, S. Iwasaki, T. Fukuhara and H. Ohkita, *ACS Appl. Mater. Interfaces*, 2021, **13**, 39322–39330.
138 Y. Yamagata, H. Benten, T. Kawanishi and M. Nakamura, *ACS Appl. Polym. Mater.*, 2021, **4**, 169–178.
139 Y. Zheng, G. J. N. Wang, J. Kang, M. Nikolka, H. C. Wu, H. Tran, S. Zhang, H. Yan, H. Chen, P. Y. Yuen, J. Mun, R. H. Dauskardt, I. McCulloch, J. B. H. Tok, X. Gu and Z. Bao, *Adv. Funct. Mater.*, 2019, **29**, 1905340.
140 Y. Li, Y. Zhang, B. Wu, S. Pang, X. Yuan, C. Duan, F. Huang and Y. Cao, *Sol. RRL*, 2022, **6**, 2200073.
141 Z. Liang, J. He, B. Zhao, M. Gao, Y. Chen, L. Ye, M. Li and Y. Geng, *Sci. China: Chem.*, 2022, **66**, 216–227.
142 T. Jia, J. Zhang, W. Zhong, Y. Liang, K. Zhang, S. Dong, L. Ying, F. Liu, X. Wang, F. Huang and Y. Cao, *Nano Energy*, 2020, **72**, 104718.
143 R. Sun, T. Wang, Q. Fan, M. Wu, X. Yang, X. Wu, Y. Yu, X. Xia, F. Cui, J. Wan, X. Lu, X. Hao, A. K. Y. Jen, E. Spiecker and J. Min, *Joule*, 2023, **7**, 221–237.
144 L. Ma, Y. Cui, J. Zhang, K. Xian, Z. Chen, K. Zhou, T. Zhang, W. Wang, H. Yao, S. Zhang, X. Hao, L. Ye and J. Hou, *Adv. Mater.*, 2023, **35**, 2208926.
145 H. Ma, J. Song, J. Qiao, B. Han, Q. Wang, M. H. Jee, L. Bu, D. Wei, H. Y. Woo, X. Hao and Y. Sun, *Energy Environ. Sci.*, 2025, **18**, 397–405.
146 Q. Bai, Y. Cheng, W. Wang, J. Chen and H. Sun, *J. Mater. Chem. A*, 2024, **12**, 16251–16267.
147 W. Qi, X. Yuan, Y. Liu, S. Yang, Y. Chu, F. Qian, L. Yan, Z. Wang, C. Duan, Q. Luo and C.-Q. Ma, *Sci. China Mater.*, 2025, **68**, 1435–1444.
148 Y. Liu, B. Liu, C.-Q. Ma, F. Huang, G. Feng, H. Chen, J. Hou, L. Yan, Q. Wei, Q. Luo, Q. Bao, W. Ma, W. Liu, W. Li, X. Wan, X. Hu, Y. Han, Y. Li, Y. Zhou, Y. Zou, Y. Chen, Y. Liu, L. Meng, Y. Li, Y. Chen, Z. Tang, Z. Hu, Z.-G. Zhang and Z. Bo, *Sci. China: Chem.*, 2022, **65**, 1457–1497.
149 H. Xu, J. Han, A. Sharma, S. H. K. Paleti, S. Hultmark, A. Yazmaciyan, C. Muller and D. Baran, *Adv. Mater.*, 2025, **37**, 2407119.